Research Article

MOLECULAR PAIN

Molecular Pain
Volume 14: 1–22

DOI: 10.1177/1744806918788648
journals.sagepub.com/home/mpx
SAGE

Therapeutic potential of Pak1 inhibition for pain associated with cutaneous burn injury

Yiqun Guo[1,2], Curtis Benson[1,2], Myriam Hill[1,2], Stefanie Henry[1,2], Philip Effraim[1,2], Stephen G Waxman[1,2], Sulayman Dib-Hajj[1,2], and Andrew M Tan[1,2]

Abstract

Painful burn injuries are among the most debilitating form of trauma, globally ranking in the top 15 leading causes of chronic disease burden. Despite its prevalence, however, chronic pain after burn injury is under-studied. We previously demonstrated the contribution of the Rac1-signaling pathway in several models of neuropathic pain, including burn injury. However, Rac1 belongs to a class of GTPases with low therapeutic utility due to their complex intracellular dynamics. To further understand the mechanistic underpinnings of burn-induced neuropathic pain, we performed a longitudinal study to address the hypothesis that inhibition of the downstream effector of Rac1, Pak1, will improve pain outcome following a second-degree burn injury. Substantial evidence has identified Pak1 as promising a clinical target in cognitive dysfunction and is required for dendritic spine dysgenesis associated with many neurological diseases. In our burn injury model, mice exhibited significant tactile allodynia and heat hyperalgesia and dendritic spine dysgenesis in the dorsal horn. Activity-dependent expression of c-fos also increased in dorsal horn neurons, an indicator of elevated central nociceptive activity. To inhibit Pak1, we repurposed an FDA-approved inhibitor, romidepsin. Treatment with romidepsin decreased dendritic spine dysgenesis, reduced c-fos expression, and rescued pain thresholds. Drug discontinuation resulted in a relapse of cellular correlates of pain and in lower pain thresholds in behavioral tests. Taken together, our findings identify Pak1 signaling as a potential molecular target for therapeutic intervention in traumatic burn-induced neuropathic pain.

Keywords

Burn injury, central nervous system, dendritic spines, pain, Pak1, preclinical, Rac1, romidepsin, synaptic plasticity, trauma

Date Received: 18 April 2018; revised: 1 June 2018; accepted: 8 June 2018

Introduction

Burn injuries and associated long-term complications are a significant public health crisis. More than 11 million individuals per year suffer burn injuries severe enough to require hospitalization and long-term care.[1] Of these patients, many develop chronic intractable pain that continues long after the initial trauma. The failure to address burn injury pain is due in part to the lack of mechanistic insight in neuropathic pain pathology and the shortage of preclinical research in the burn-injured population.[2–6] It has been suggested that chronic pain following burns may arise from excessive neuronal activity within scar tissue, poorly regenerated nerve endings, inflammation, and central mechanisms.[7–9] Opioid resistance observed in burn patients may also be due to maladaptive structural plasticity within the central nervous system (CNS).[1] Importantly, emerging evidence suggests that dendritic spines may be an "actionable" morphological correlate for addressing chronic neurological disease, for example, pain.[10,11]

We have previously documented in several studies that dendritic spine dysgenesis in the nociceptive neurons in the dorsal horn accompanies central sensitization

[1]Department of Neurology, Center for Neuroscience and Regeneration Research, Yale University School of Medicine, New Haven, CT, USA
[2]Rehabilitation Research Center, Veterans Affairs Connecticut Healthcare System, West Haven, CT, USA

Corresponding Author:
Andrew M Tan, Center for Neuroscience and Regeneration Research, 127A, 950 Campbell Avenue, Building 34, West Haven, CT 06516, USA.
Email: andrew.tan@yale.edu

and neuropathic pain.[12,13] In experimental burn injury, dendritic spines change to a dysgenic state in a Rac1-dependent manner. Inhibition of Rac1 suppresses dendritic spine dysgenesis and attenuates neuropathic pain.[14] Cessation of Rac1 inhibition permits a relapse in both dendritic spine dysgenesis and abnormal pain.[11]. As a clinical target, however, Rac1 has low therapeutic utility due to its complex intracellular dynamics.[15–17] Thus, in this study, we sought alternative druggable targets and identified Pak1 as a potentially useful therapeutic target for addressing pain.[11,13] Pak1 is a Rac1 effector kinase that links Rac1 signaling to cytoskeletal reorganization underlying dendritic spine plasticity. Although Pak1 has been implicated in a spectrum of neurological diseases and disorders,[18–21] this kinase has not been studied in mechanisms underlying neuropathic pain.[22–24]

We hypothesized that inhibition of Pak1 activity will disrupt abnormal dendritic spine remodeling and reduce neuropathic pain in a second-degree burn injury model. We performed longitudinal experiments that investigated dendritic spine profiles in burn injury-induced pain: (1) without treatment, (2) during treatment, and (3) following withdrawal of treatment with romidepsin, an FDA-approved Pak1 inhibitor. Our findings demonstrate that after burn injury, mechanical and heat pain increase along with dendritic spine dysgenesis in the ipsilateral dorsal horn. Expression of c-fos, a marker for neuronal activity, also increases, suggesting that there are post-burn increases in central nociceptive activity. Pak1-inhibition by romidepsin decreased dendritic spine dysgenesis, reduced c-fos expression, and partially rescued pain thresholds. Romidepsin cessation allowed cellular pain correlates and neuropathic pain to return. Together, our data demonstrate that Pak1 signaling is a potential molecular target for addressing traumatic burn injury-induced neuropathic pain and highlight an opportunity of repurposing clinically available drugs to expedite development of novel pain therapies.

Methods

Animals and burn injury

Experiments were performed in accordance with the National Institutes of Health *Guidelines for the Care and Use of Laboratory Animals* and were approved by the VA Institutional Animal Use Committee. Animals were housed under a 12-h light/dark cycle in a pathogen-free area with food and water provided ad libitum. Weight-matched, adult mice were used for this study (male/female equal mix; C57Bl6; 25 ± 1.8 g; Harlan, Indianapolis, IN). A total of 47 animals were included in the final analysis of this study. To produce the second-degree burn injury, we used modified procedures described previously.[14,25] The burn apparatus was custom designed in Fusion 360 (Autodesk) and three-dimensional (3D) printed on an Ultimaker 2+ printer (Ultimaker, Netherlands) using heat-resistant *acrylonitrile butadiene styrene* (ABS) filament (Figure 1(a)). Heated water (75°C) was continuously pumped through an inflow opening in the apparatus, whereby it heated a copper plate (1 mm thick), and exited through an outflow pipe. To ensure consistent heat was applied animal-to-animal, we also monitored the temperature of the metal plate with a surface thermometer. After establishing baseline withdrawal thresholds (Figure 2), animals were briefly anesthetized with isoflurane (2%–3% vaporized in oxygen). The glabrous surface of the left hind paw was applied to the 75°C heated metal surface of the apparatus for 15 s. To maintain consistent pressure across animals between the plantar skin and metal surface, we placed a 10-g-weighted sandbag onto the dorsal aspect of the paw. This injury

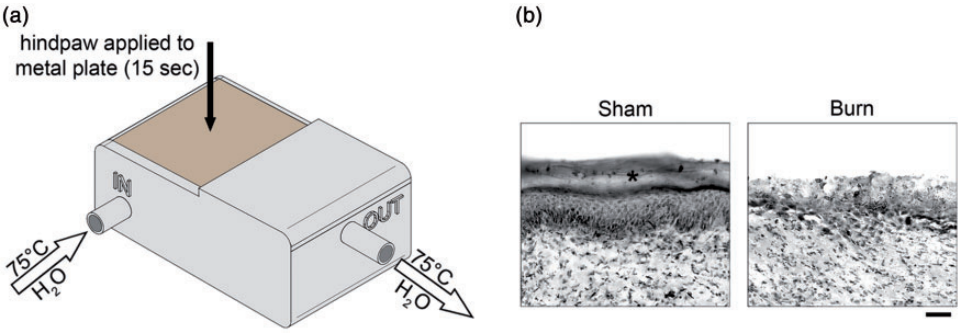

Figure 1. Partial thickness burn injury model. To produce the second-degree burn injury, we used a modified procedure described previously.[14,25] (a) The burn apparatus was custom designed, comprises a 3D-printed chamber, and attached copper metal plate (heated surface). To maintain consistent temperature, heated water (constant 75°C) was continuously pumped through the inflow into the chamber and exited through an outflow pipe. Under anesthesia, the glamorous surface of the hind paw was applied to the heated plate and held for 15 s with a 10-g weight. (b) This burn model reliably produces epidermal skin damage (*) into the deeper dermis layer, an injury profile indicative of a second degree, partial thickness burn. Scale bar in (b) is 200 μm.

model produces a burn injury of approximately 20% to 25% of the plantar surface area and a burn injury site skin blister indicative of a second-degree burn injury.[14] To prevent infection, silver sulfadiazine ointment was applied to the injured site. Sham animals underwent the same procedures, but the metal surface temperature was maintained at room temperature ($24 \pm 1°C$). Anti-Pak1 or control treatment consisted of dimethyl sulfoxide (DMSO) (1% in 0.01 M phosphate-buffered saline (PBS)) or romidepsin (Abcam, ab143287, 5 mg/kg in 1% DMSO/0.01 M PBS), respectively, that was injected intraperitoneally (i.p.) over three days at 9:00 a.m. everyday successively on Days 4, 5, and 6 post-burn and before any behavioral testing (Figure 2). The dosage of romidepsin was initially calculated using the FDA guidelines for converting clinical drug dosages between human and animal (animal mg/kg dose × animals surface area (km) = human mg/kg dose × human surface area (km)) from the maximum tolerated dose (MTD) for romidepsin for human cancer treatment (https://www.fda.gov/downloads/drugs/guidances/ucm078932.pdf; accessed 18 March 2018). Based on a pilot dose–response study (data not shown), the MTD for romidepsin use in our animals was 5 mg/kg injected i.p. twice daily. These procedures resulted in the production of five comparator groups: Sham + DMSO, Burn + anti-Pak1 (Day 6), Burn + DMSO (Day 6), Burn + DMSO (Day 10), and Burn + anti-Pak1 (Day 10) (Figure 2).

Behavioral testing

A blinded experimenter performed behavioral experiments in a dedicated testing room under invariant conditions at room temperature ($23 \pm 2°C$). All behavioral testing was performed at seven-time points: baseline (before burn injury), Days 3, 4, 5, 6, 7 and 10 after burn injury. To assess whether romidepsin treatment had significant effects on gross locomotor or motivational/affective function, we performed additional tests (shown in Figure 3). These studies were all performed before pain-related behavioral testing (Figure 10). To evaluate muscle strength and mobility with all four limbs, we used a modified Kondziela's inverted screen test.[26] The mesh was made of 1-mm-thick metal wire with a 12-mm square pattern. After the subject was placed upright in the center of the mesh screen, the mesh was rotated to an inverted position over a 2-s period, with the head declining first. This position was held until the animal let go of the mesh and fell. The latency from the mesh inversion to the animal falling off was recorded. The maximum latency was capped at 120 s. Normal mice generally score the maximum latency

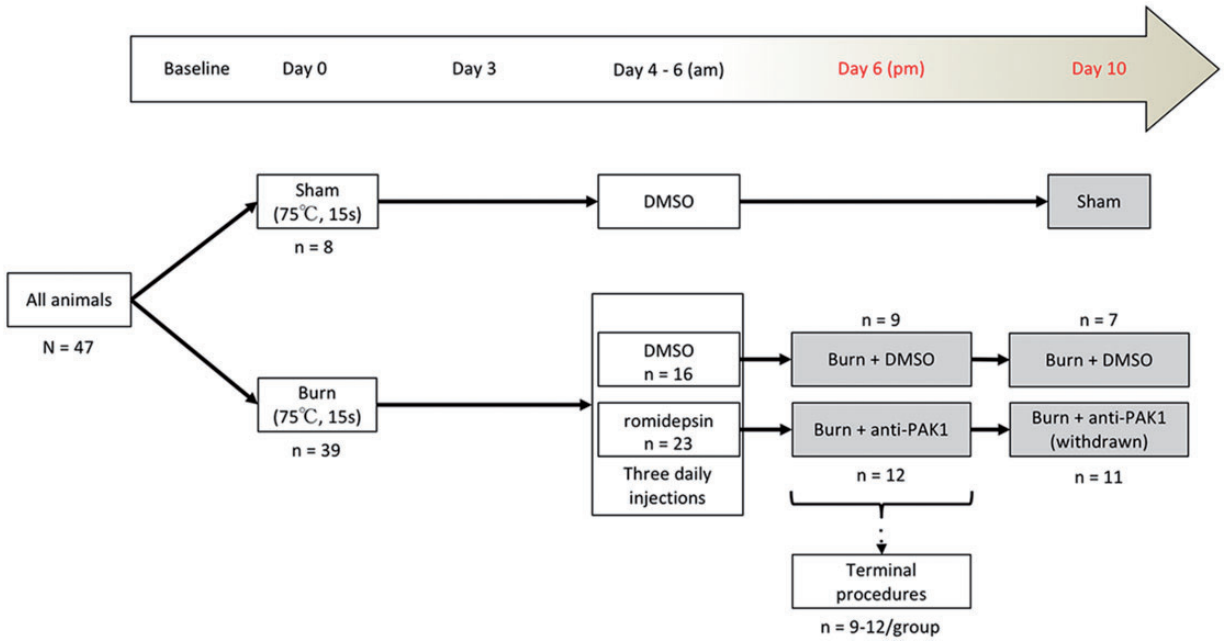

Figure 2. Study design. Animals (n = 47) we weight-matched and randomly assigned to Sham or burn-injured groups. On Day 0, animals either received a burn injury or control Sham (no burn) procedure. After a recovery period, animals were administered with DMSO vehicle or romidepsin injected intraperitoneally for three consecutive days at 9:00 a.m. (Days 3, 5, and 6). These procedures produced five comparator groups: Sham + DMSO, Burn + anti-Pak1 (Day 6), Burn + DMSO (Day 6), Burn + DMSO (Day 10), and Burn + anti-Pak1 (Day 10) (gray boxes). All functional testing was performed in the afternoon (p.m.) at baseline, Days 3, 4, 5, 6, 7, and 10. Terminal procedures for tissue collection were performed immediately following functional testing at endpoint Day 6 or Day 10. DMSO: dimethyl sulfoxide.

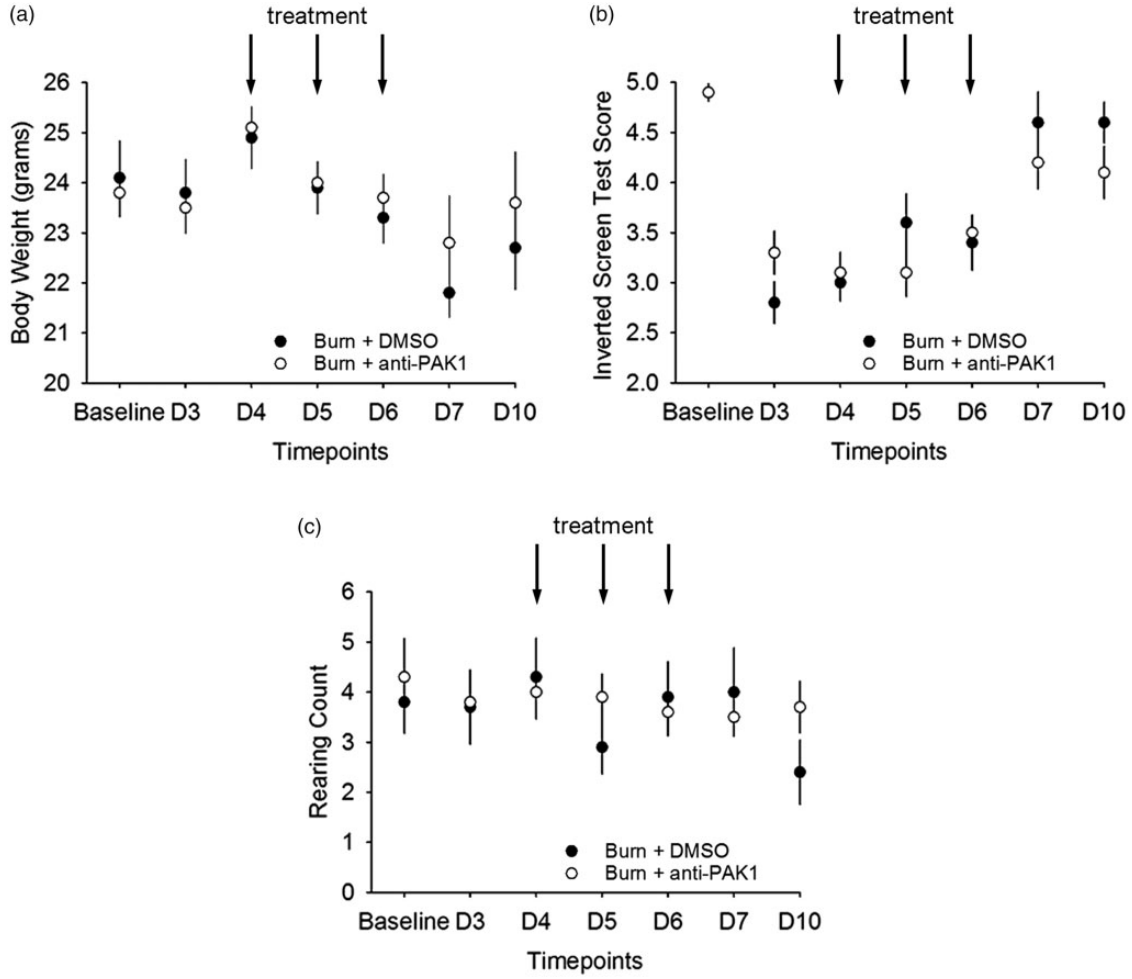

Figure 3. Romidepsin treatment at maximum tolerated dose does not have adverse effects on overall animal well-being. To assess whether romidepsin effects (a) body weight, (b) gross locomotor function, and (c) motivational/affective function, we performed several behavioral studies over the experimental period. We did not observe any differences in any of these behavioral tests at any time point before, during, or after romidepsin and DMSO treatment. DMSO: dimethyl sulfoxide.

on this task, as reported previously (Deacon, 2013). For analysis, latency was scored on a scale from 1 to 5 (worst-to-best; 1: 1–10 s; 2: 11–25 s; 3: 26–60 s; 4: 61–90 s; and 5: 91–120 s). The mesh was cleaned with soap and water and dried between each animal testing trial. To assess affective/motivational/exploratory behavior, hind limb rearing behaviors were assessed over the experimental study period. Mice were placed into an empty Plexiglas box and allowed to freely move during a 3-min observation period. The number of rearing behaviors was measured. A single rearing event was defined as a behavioral event when an animal stood only on its hind limbs and rested at least one of its forelimbs on the Plexiglass wall of the box. Romidepsin has the potential to adversely affect appetite. To ensure our romidepsin dosage did not lead to significant adverse effects on overall animal well-being that could confound our behavioral studies, we measured and compared body mass (g) across animal groups following all behavioral testing.

For pain-related behavioral testing, after acclimation to the testing area (60 min), mechanical sensory thresholds were determined by paw withdrawal in response to a graded series of Von Frey filaments (Stoelting, Wood Dale, IL, USA). Filaments were applied to the metacarpal area on the glabrous surface of the left hind paw, avoiding the damaged skin/scar area of the burn site.[8,14] The testing area was consistent across animals. We used a modification of the Dixon "up-down" method to determine mechanical nociceptive threshold.[27] For assessing heat withdrawal threshold, we used the Hargreaves' testing method whereby paw withdrawal latency was measured in response to a radiant heat source.[28,29] After acclimation in the testing area for 60 min at ambient room temperature ($23 \pm 2^{\circ}C$), animals were placed in Plexiglass box situated on an elevated

glass plate (University of California San Diego, Anesthesiology Department, La Jolla, CA). A radiant heat source heated the glass plate directly under the glabrous surface of the paw. Upon paw withdrawal, the heat source was automatically turned off and the latency (seconds) recorded. To prevent tissue damage, heat was automatically turned off at 20.5 s.

Histology

To preserve any effects of drug treatments or activity-dependent antigen-tissue expression, we rapidly euthanized animals following pain behavioral testing (within 20 min) at experimental endpoints on Day 6 or Day 10. Mice were anesthetized using a mixture of ketamine/xylazine (100/10 mg/kg, i.p.) and intracardially perfused with 4% paraformaldehyde (0.01 M PBS) and cryoprotected in 30% sucrose. Spinal lumber enlargement (L3–L5) and spleen tissue was collected for post-mortem analysis. For immunohistochemistry, 20-μm-thick tissues were cut on a cryostat (Leica; Bannockburn, IL) and mounted on Superfrost+ slides (Fisher Scientific; Pittsburg, PA). Briefly, sections were blocked in 4% normal donkey serum (in 2% bovine serum albumin; 1% Triton-X100; 0.02% Na azide; 0.01 M PBS) and incubated overnight in antibodies (monoclonal Alexa Fluor® 488 conjugated NeuN (1:500, MAB377X), Chemicon), rabbit polyclonal Acetyl-Histone H3 (1:200, 06–942, Chemicon), rabbit polyclonal Pak1 (1:200, #2602, Cell Signaling Technology), rabbit polyclonal Rac1 (1:200, ab155938, Abcam), goat polyclonal p-Raf-1 (Ser 338; 1:200, sc-12358, Santa Cruz), rabbit polyclonal c-fos (1:200, sc-52, Santa Cruz), rabbit monoclonal Iba-1 (1:200, 019–19741, Wako), chicken polyclonal glial fibrillary acidic protein (GFAP) (1:200, ab4674, Abcam) Tissue sections were washed in 0.01 M PBS and incubated in appropriate secondary antibodies (donkey anti-goat, Alexa 555; donkey anti-rabbit, Alexa 555; donkey anti-chicken, Alexa 488). Coverslips were applied using anti-fade gel/mount (BioMeda, Foster City, CA). Immunofluorescent images were captured using a Nikon Eclipse E800 microscope with an Andor camera (DR 328G-C01-SIL, Andor Technology LTD, Olympus America Inc).

For tissue analyses, background signal was equalized across all samples.[30,31] A blinded investigator quantified fluorescent expression of target proteins using Image J software (National Institutes of Health software download: http://rsbweb.nih.gov/ij/) in the dorsal horn and normalized these values with Sham values (i.e., mean of Sham data/X data, where X is the raw data value). Data were then averaged within groups and compared across groups. For the analysis of c-fos expression in the dorsal horn, we divided the dorsal horn into two dorso-ventral regions using methods and criteria described previously[30,31]: dorsal (laminae I–III) and intermediate zone (IV–V). C-fos immunoreactive cells were counted, averaged within groups, and compared across treatment groups.

To visualize dendritic spines, mice were prepared for Golgi-cox staining.[11] Golgi staining permits sampling of a large number of neurons with detailed resolution of dendritic spines and permits full reconstructions of whole neurons, including ultra-fine processes. This Golgi-impregnated tissue is also impervious to long exposure to high-intensity light that would otherwise diminish other labeling systems, for example, fluorophores. Briefly, mice were killed by decapitation without fixation. Spinal cord tissues from the lumbar enlargement (L4–L5) were rapidly dissected (<5 min), rinsed in distilled water, and processed using a commercial kit (using manufacturer's instructions (FD Neurotechnologies, Ellicott, MD) (Sham + DMSO, n = 4; Burn + DMSO, Day 6, n = 4; Burn + DMSO, Day 10, n = 3; Burn + romidepsin, Day 6, n = 4; Burn + romidepsin, Day 10, n = 5). Twenty-days after incubation in the kit's impregnation solutions, 180-μm-thick coronal sections were cut on a vibratome (Leica VT1200S; Leica Biosystems, IL) and mounted on gelatinized glass slides. Mounted sections were stained, rinsed in distilled water, dehydrated, cleared, and coverslipped using Permount medium. Golgi-stained sections were visualized with a transmitted light microscope (Nikon Eclipse 80i). Images were captured with a HQ Coolsnap camera (Roper Scientific; Tucson, Arizona).

Dendritic spine analysis

Digital reconstructions were rendered and analyzed by blinded investigator using a Neurolucida software suite (version 9.0; Microbrightfield, Williston, VT) and pen tablet (Intuos 5 touch, Wacom).[11] For our purposes, we sampled wide-dynamic range (WDR) neurons in the lumbar enlargement located in the intermediate zone (laminae IV–V, ~500–800 μm deep). To identify and sample WDR neurons for analysis, we used a sampling workflow consisting of five inclusion criteria[11,32]: (1) neurons were located in Rexed lamina IV/V; (2) stained neurons must have dendrites and spines that are impregnated and appeared as a continuous length; (3) at least one dendrite extended into an adjacent lamina relative to the origin of the cell body; (4) at least half of the primary dendritic branches remained within the thickness of the tissue section, such that their endings were not cut and instead tapered into an ending; and (5) the soma diameter was greater than 25 μm. To ensure there were no morphological differences across our sampled neurons, we used NeuroExplorer software (Microbrightfield, Williston, VT) to measure maximum cell diameter, total dendritic

Table 1. Comparisons of sampled neuronal attributes.

	Maximum diameter	Total dendrite length (μm)	No. of primary dendrites	Mean length of primary dendrites (μm)	Primary dendrites with secondary branches (%)
Sham	40.5 ± 12.8	683.2 ± 585.5	4.4 ± 0.75	157.6 ± 251.5	34.0 ± 20.3
Burn + DMSO (Day 6)	51.4 ± 19.5	771.8 ± 264.9	5.1 ± 1.7	157.7 ± 221.0	42.8 ± 27.4
Burn + anti-Pak1 (Day 6)	39.9 ± 15.8	874.7 ± 541.7	5.2 ± 1.7	103.4 ± 101.1	37.9 ± 19.8
Burn + DMSO (Day 10)	40.7 ± 11.9	620.3 ± 290.0	4.6 ± 1.4	97.3 ± 77.8	39.4 ± 21.6
Burn + anti-Pak1 (Day 10 withdrawn)	38.8 ± 9.3	598.0 ± 284.2	4.7 ± 1.0	96.8 ± 71.1	38.2 ± 18.0

Note: Data shown as mean ± standard deviation. DMSO: dimethyl sulfoxide.

branch length, number of primary dendrites, mean length of primary dendrites, and the percentage of primary dendrites with secondary branches (Table 1). These morphological attributes were measured and compared across animals and treatment groups post hoc and control for the morphological diversity of spinal cord dorsal horn neurons. We identified a total of 127 neurons for inclusion in our analysis (Sham = 14; Burn + DMSO, D6 = 28; Burn + DMSO, D10 = 20; Burn + romidepsin, D6 = 35; Burn + romidepsin, D10 = 30). To ensure that dendritic spines were accurately sampled, we used specific morphological characteristics defined previously.[33] We defined a dendritic spine neck as the structure juxtaposed between the parent dendrite branch and the base of the spine head, which appears as a distal swelling into a bulb-like structure. Thin- and mushroom-shaped spines were classified: thin spines had head diameters that were less than or equal to the length of the spine neck, whereas mushroom spines had head diameters that were greater than the length of the spine neck. The use of these geometric categories permitted us to use simple but very explicit rules for classifying spine morphology. Note that although this approach precluded discrimination of other subtle variations in spine shape, we were previously able to collect a very large sample size that has permitted us and others to link the physiological characteristics of thin- and mushroom-shaped spines with neurophysiological circuit function.[34–39] We are aware that spine criteria in this study do not have direct implications for physiological characterization of the neurons we analyzed but were used to control for the morphological diversity within the sampled neuronal population. To reconstruct sampled neurons, we used Neurolucida software and analyzed the complete three-dimensional reconstructions of dorsal horn neurons.[11] Dendritic spine density was expressed as spine number per 10-μm dendritic length. To determine any changes in the spatial distribution of spines, we used a Sholl's analysis.[24] Seven 50-μm-wide spherical bins were formed around each cell body, spine density within each bin was averaged within each treatment group, and mean data were compared against equivalent bins across groups.

Statistical analysis

All statistical tests were performed at the α-level of significance of 0.05 by two-tailed analyses using parametric or non-parametric test, as appropriate. We used measures analysis of variance (ANOVA) and Kruskal–Wallis one-way ANOVA on ranks, followed by Bonferonni's or Dunn's post hoc analysis, respectively. Data management and statistical analyses were performed using SigmaPlot (version 12.5; Systat Software Inc.) and Microsoft Office Excel (2011). Data in the text are described as mean ± standard deviation. All graphs are plotted as mean ± SEM using SigmaPlot.

Results

Romidepsin administration does not have adverse effects on overall animal well-being. We administered romidepsin systemically using the MTD (5 mg/kg i.p. twice daily for three days) determined in a pilot dose-escalation study (data not shown). To ensure that treatment with romidepsin did not produce adverse effects that could potentially confound our pain assessments, we monitored three outcome measures during the time course of the study: (1) body weight, (2) a modified Kondziela's inverted screen test,[26] and (3) affective/exploratory rearing behavior (Figure 3).

The most common adverse events observed in human studies of romidepsin (nausea, loss of appetite, change in taste sensation, lack of strength, fatigue, and diarrhea) can directly impact body weight

(http://www.celgene.com/content/uploads/istodax-pi.pdf). Therefore, we monitored body weight of animals treated with romidepsin or DMSO vehicle (Figure 3(a)). We did not observe differences in animal body weight after treatment with romidepsin ($p > 0.05$; baseline vs. Days 3, 4, 5, 6, 7, and 10: range across all groups, 20.3–27.4 g), or compared with DMSO treatment ($p > 0.05$; vs. any testing day: range 18.7–26.9 g).

To assess general muscle strength and mobility with all four limbs, we performed an inverted screen test.[26] In this test, animals are placed on a wired mesh, which is then inverted. Latency-to-fall scores were categorized into a 1 to 5 ordinate scale from worst-to-best (1: 1–10 s; 2: 11–25 s; 3: 26–60 s; 4: 61–90 s; 5: 91–120 s) (Figure 3(b)). At baseline, before burn injury, animals in either romidepsin or DMSO treatment group had similar inverted mesh scores ($p > 0.05$; 4.9 ± 0.42 vs. 4.9 ± 0.25). Following burn injury, all animals exhibited decreased inverted mesh scores as compared with baseline without injury, suggesting that burn injury compromised these animals' ability to hold onto the mesh after it was inverted ($p < 0.05$; from a baseline mean of 4.9 down to the lowest score of 3.0 or 3.1 in DMSO or romidepsin-treated animals, respectively). Burn-injured animals with DMSO or romidepsin treatment had similar inverted mesh scores when compared on each testing day ($p > 0.05$; Days 3, 4, 5, 6, and 10: range 2.0–5.3).

Rearing behavior is associated with general activity level and has been used as a measure of higher order, cognitive-affective/exploratory function in animal models (i.e., more rearing events indicates higher levels of general activity and exploration).[40–42] To test rearing, animals were placed into an enclosed box and allowed to freely explore the chamber for a 3-min observation period (see "Methods" section) (Figure 3(c)). In all comparisons, animals exhibited a similar number of rearing events at baseline, before or after burn injury, and with romidepsin or DMSO treatment at any testing day ($p > 0.05$: range across all groups and testing days: 2.8–6.8). Taken together, these data demonstrate romidepsin treatment has no detectable effects on established measures of animal overall well-being and function.

Romidepsin is bioavailable and exerts a detectable action in the spinal cord dorsal horn

To assess the bioavailability of romidepsin, we assessed the expression of two biomarkers for drug-tissue response: histone acetylation and p-Raf (Figure 4). Romidepsin is a histone deacetylase (HDAC) inhibitor, which leads to a potent block of Pak1 kinase activity. As such, an established clinical index for romidepsin tissue response is increased histone acetylation in exposed tissue.[43,44] We assessed histone acetylation in both spleen and spinal cord tissue of burn-injured or control animals on Day 6 (immediately after the last drug dose) and Day 10 (following drug withdrawal) (Figure 4(a) to (c)). In spleen (Figure 4(a)), we observed a significant increase in histone acetylation with romidepsin treatment as compared with DMSO vehicle on Day 6 post-burn (D6: $p < 0.05$, 1.17 ± 0.10 vs. 1.06 ± 0.13 normalized expression, ANOVA on ranks) (Figure 4(d)). As expected on Day 10, after drug withdrawal, we observed no difference in spleen histone acetylation across any burn-injured group with DMSO or romidepsin treatment (D10: 1.0 ± 0.15 vs. 1.1 ± 0.08 normalized expression), demonstrating that the effect of romidepsin had worn off. Additionally, we found no significant difference in spleen histone acetylation in any burn-injured group at Day 10, with DMSO or romidepsin treatment, as compared against Sham (at D6: 1.0 ± 0.11). Together, these results demonstrate that the effect of treatment with romidepsin is short-lived, with histone acetylation levels returning to untreated post-burn levels after drug discontinuation.

In spinal cord tissue (Figure 4(e)), we observed a significant increase in histone acetylation in neurons, which were marked by immunostaining with the neuron-specific marker, NeuN, following romidepsin treatment as compared with DMSO treatment on Day 6 (D6: $p < 0.05$, 1.1 ± 0.15 vs. 1.01 ± 0.10 normalized expression, ANOVA on ranks). On Day 10, following drug treatment withdrawal, we found no difference in histone acetylation levels in comparisons across either romidepsin or DMSO-treated burn-injured animals (D10: 0.98 ± 0.04 vs. 0.95 ± 0.04 normalized expression), or when compared against Sham (at D10: 1.0 ± 0.07). These findings demonstrate that systemically delivered romidepsin can penetrate the blood–brain barrier (BBB) into the spinal cord and affect neuronal tissue. Treatment withdrawal data further demonstrates that the effect of romidepsin is transient, that is, the levels of histone acetylation returns to Sham levels following the discontinuation of romidepsin treatment.

To further assess the bioavailability of romidepsin, we measured the expression of p-Raf following burn injury (Figure 4(c) and (f)). Raf-1 is a downstream effector of Pak1, and romidepsin activity in a tissue would result in a decrease of activated Raf-1, that is, phosphorylation of Ser338 on Raf-1, or p-Raf expression.[45,46] On Day 6 after burn injury, we observed a significant decrease in p-Raf expression in neurons with romidepsin treatment as compared with DMSO (D6: $p < 0.05$, 0.93 ± 0.01 vs. 0.97 ± 0.01 normalized expression, ANOVA on ranks) (Figure 4(f)). On Day 10, drug discontinuation resulted in no detectable difference in p-Raf expression between burn-injured animals treated with romidepsin or DMSO (D10: 0.96 ± 0.01 vs. 0.98 ± 0.001 normalized expression). In comparisons against Sham (at D6: 1.0 ± 0.07), we also observed no significant difference with burn-injured groups on Day 6 or Day 10, with DMSO or romidepsin treatment.

Romidepsin decreases burn injury-induced c-fos expression

The immediate early gene *c-fos* has been established as a molecular marker of neural activity in spinal cord

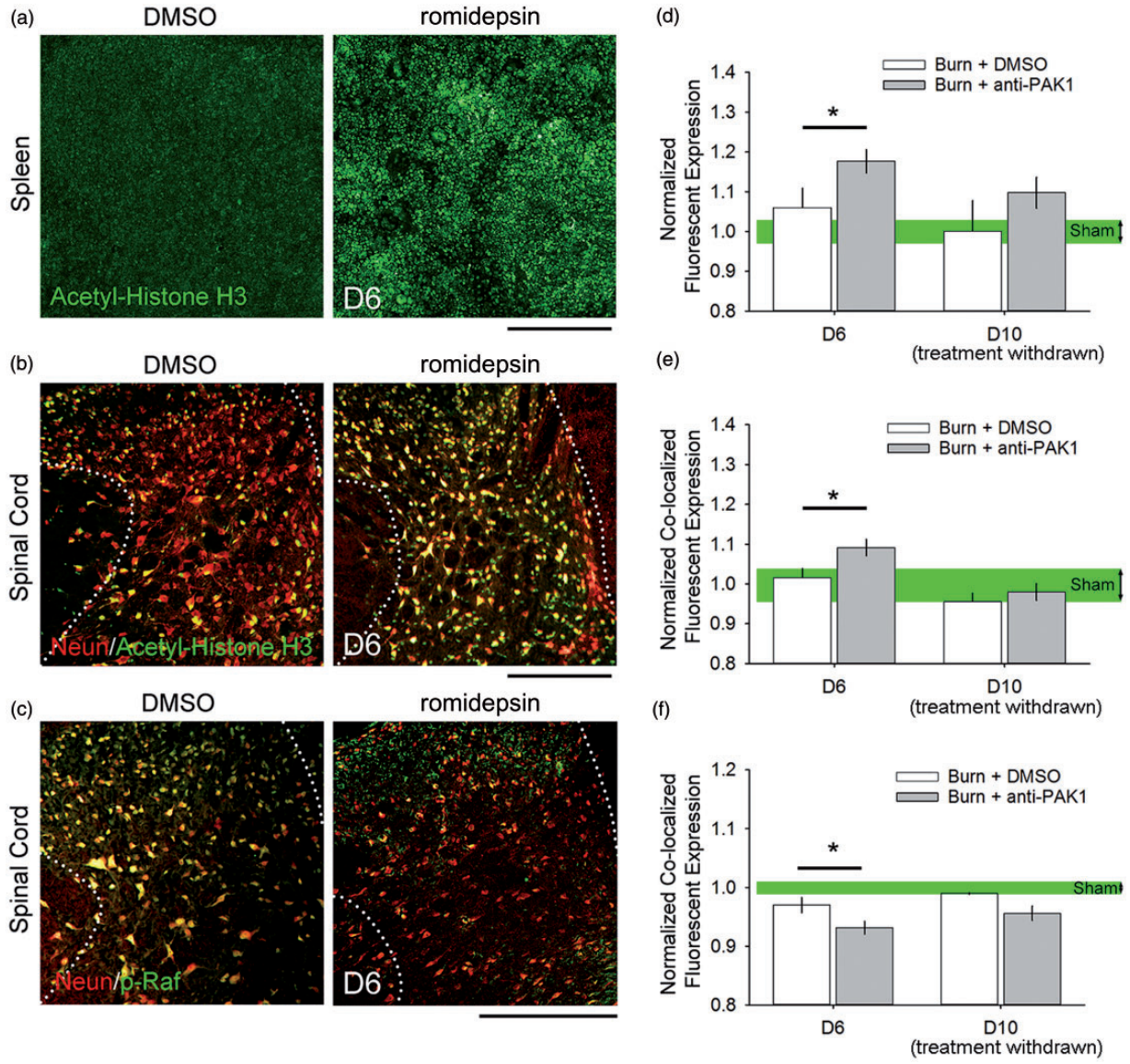

Figure 4. Romidepsin has bioavailability and tissue action in the spinal cord. To assess the bioavailability of romidepsin through our study, we measured the expression of biomarkers for drug-tissue response in the spleen and spinal cord at Day 6 (<24 h after treatment) and Day 10 (after drug withdrawal). At Day 6, we observed an increase in histone acetylation in the (a, d) spleen and (b, e) neurons in the spinal cord dorsal horn (co-localized immunoreactivity of acetyl-histone H3 with NeuN), as compared with DMSO treatment (*$p < 0.05$). At Day 10, there was no difference in histone acetylation between burn-injured treatment groups ($p > 0.05$). Additionally, on Day 6, we observed (c, f) a decrease in Pak1 effector, p-RAF, expression in neurons in the spinal cord dorsal horn (*$p < 0.05$). There was no difference in p-RAF expression on Day 10 following drug withdrawal ($p > 0.05$). In comparisons with Sham, we observed no difference in biomarker expression levels in burn-injured animals at any time point ($p > 0.05$). Scale bars in (a) to (c) are 500 μm. Graphs are mean ± SEM. DMSO: dimethyl sulfoxide.

neurons. In burn injury models, c-fos expression increases in association with increased pain outcome.[25,47] To assess c-fos expression as a result of burn injury with or without romidepsin, animals were rapidly processed for tissue collection within <30 min after behavioral thermal pain testing at experimental endpoints on Day 6 or Day 10. Increased c-fos expression appeared in both DMSO and romidepsin-treated burn-injured animals within the dorsal horn of the spinal cord, as shown in Figure 5(a) and (b), respectively. In the superficial dorsal horn (lamina I–III), all burn-injured animal groups demonstrated significantly greater c-fos expression, as compared with Sham at Day 6 (D6: $p < 0.05$, DMSO or romidepsin vs. Sham; 28.8 ± 4.9 or 26.6 ± 1.8 vs. 22.7 ± 1.6 c-fos+ cells, ANOVA on ranks with Dunn's post hoc) and Day 10 (D10: 26.1 ± 2.9 or 27.6 ± 4.8 vs. 22.7 ± 1.6 c-fos+ cells) (Figure 5(c)). In the intermediate zone (lamina IV–V), however, c-fos

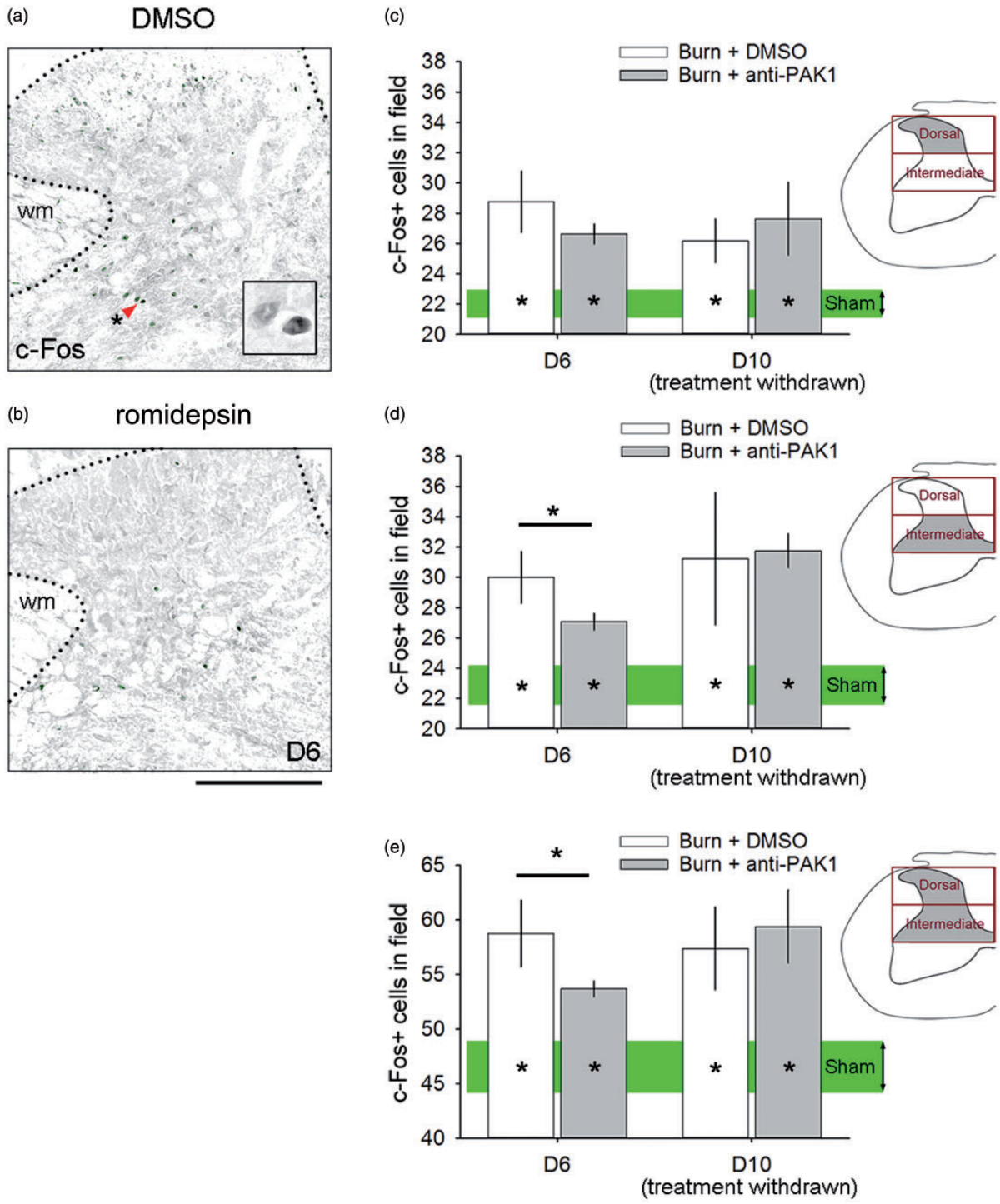

Figure 5. Romidepsin decreases c-fos expression. Expression of c-fos was assessed in the dorsal horn following burn injury treated with (a) DMSO or (b) romidepsin, and compared with Sham levels. (C) In the superficial dorsal horn (lamina I–III), all burn-injured animals had significantly greater c-fos expression as compared with Sham at Day 6 or Day 10 (*$p < 0.05$). (d) In the intermediate zone (lamina IV–V), c-fos expression decreased with anti-Pak1 romidepsin treatment as compared with DMSO (*$p < 0.05$). We observed a significant difference at Day 10 following drug withdrawal ($p > 0.05$). In all comparisons against Sham, all burn-injured animals had greater c-fos expression in the intermediate zone at Day 10 (*$p < 0.05$). (e) In total, within the superficial dorsal horn and intermediate zone, burn-injured animals treated with either DMSO or romidepsin at Day 6 and Day 10 had significantly greater c-fos expression as compared with Sham (*$p < 0.05$). Treatment with romidepsin at Day 6 significantly reduced c-fos expression within these laminae (I–V) of the dorsal horn (*$p < 0.05$). Scale bars in (a) and (b) are 500 μm. Graphs are mean ± SEM. DMSO: dimethyl sulfoxide.

immunoreactive cells were significantly decreased in burn-injured animals with romidepsin treatment as compared with DMSO at Day 6 (D6: 27.1 ± 1.5 vs. 29.9 ± 4.1 c-fos+ cells, ANOVA on ranks with Dunn's post hoc). By Day 10 following drug withdrawal, the differences between romidepsin and DMSO treatment diminished, and we observed no difference between burn-injured animal groups (D10: 31.8 ± 2.2 vs. 31.2 ± 8.7 c-fos+ cells). In all comparisons against Sham, burn-injured animals continued to have significantly greater c-fos expression in the intermediate zone at Day 10 ($p < 0.05$, D10 Sham: 23.8 ± 2.3, ANOVA on ranks with Dunn's post hoc) (Figure 5(d)). In all comparisons of c-fos expression in both the superficial and intermediate zone of the dorsal horn (i.e., combined lamina I–V), burn-injured animals treated with DMSO or romidepsin at Day 6 and Day 10 had significantly greater c-fos expression than Sham (D6: $p < 0.05$, DMSO or romidepsin vs. Sham; 58.8 ± 7.4 or 53.7 ± 2.1 vs. 46.5 ± 3.7 c-fos+ cells, ANOVA on ranks with Dunn's post hoc; D10: $p < 0.05$, DMSO or romidepsin vs. Sham; 57.4 ± 7.5 or 59.4 ± 6.7 vs. 46.5 ± 3.7 c-fos+ cells, ANOVA on ranks with Dunn's post hoc) (Figure 5(e)). Treatment with romidepsin at Day 6 significantly reduced c-fos expression within these laminae (I–V) of the dorsal horn (D6: $p < 0.05$, DMSO vs. romidepsin; 58.8 ± 7.4 vs. 53.7 ± 2.1 c-fos+ cells, ANOVA on ranks with Dunn's post hoc). Taken together, these results demonstrate that romidepsin treatment after burn injury can rapidly and transiently attenuate c-fos expression (i.e., a marker for neuronal activity) within the intermediate zone, a region that receives diverse sensory input from low- and high-threshold afferents.

Increased dendritic spine density accompanies burn injury

Our previous work has shown that abnormal dendritic spine profiles contribute to neuropathic pain in rat models of injury or disease.[11,13,14] To assess the changes in dendritic spine morphology in our model of second-degree burn injury, we analyzed Golgi-stained spinal cord tissue from the lumbar enlargement (L4–L5) (Figure 6(a)). WDR neurons were identified based on morphological criteria (see "Methods" section). All sampled neurons had cell bodies that were completely within the intermediate zone (laminae IV–V) and clearly visible dendritic trees (Figure 6(b)). As shown in Figure 6(c), dendritic spine protrusions appear along dendrites. Dendritic spine morphologies qualitatively differ across Sham and burn-injured animals and across time between Day 6 and Day 10. To control for any sampling variation in gross cell morphology prior to dendritic spine analyses, we compared additional morphological attributes of sampled neurons, including cell body diameter, total dendritic branch length (i.e., all projections), the number of primary dendrites (i.e., those that project directly from the cell body), the average length of the primary dendrite, and the percentage of primary dendrites with secondary branches (Table 1). We did not observe any differences in these attributes in comparisons across any treatment group, or over time, between Day 6 and Day 10 endpoints ($p > 0.05$ for all comparisons). This supported our interpretation that any observed differences in dendritic spine profiles were not due to variations in neuronal sampling.

Our previous work has identified a common motif of dendritic spine morphology on dorsal horn neurons that strongly associates with nociceptive hyperexcitability in the dorsal horn and neuropathic pain, including (1) increased dendritic spine density and (2) a redistribution of dendritic spines toward branch regions located closer to the cell body.[11] To obtain an accurate profile of dendritic spines from spinal cord tissue, we reconstructed Golgi-stained WDR neurons using a Neurolucida software system (Figure 7(a) to (e)). Dendritic spines were mapped along each reconstructed neuron and color-coded according to their structural classification: thin-shaped spines (blue dots) or mushroom-shaped spines (red dots). A total of 125 neurons were rendered and included in the final analyses.

As shown in Figure 8(a), on Day 6, all burn-injured animals treated for three days with DMSO ($n = 27$) or romidepsin ($n = 34$) demonstrated significantly increased total dendritic spine density as compared with Sham ($n = 14$) (D6: $p < 0.05$, 3.5 ± 0.6 or 2.8 ± 0.4 vs. 2.4 ± 0.4 total spines per 10-μm dendrite length, one-way ANOVA with Bonferroni's post hoc). Romidepsin treatment in burn-injured animals significantly reduced total dendritic spine density as compared with DMSO treatment at this time point ($p < 0.05$, 3.5 ± 0.6 vs. 2.8 ± 0.4 total spines per 10-μm dendrite length, one-way ANOVA with Bonferroni's post hoc). By Day 10 following drug withdrawal, total dendritic spine density in romidepsin-treated animals approached the density profiles observed with DMSO-treated animals with burn injury ($p > 0.05$). At this time point, both burn-injured animal groups treated with DMSO ($n = 20$) or romidepsin ($n = 30$) continued to have significantly increased total dendritic spine densities as compared with Sham (D10: $p < 0.05$, 3.1 ± 1.1 or 2.9 ± 0.6 vs. 2.4 ± 0.4 total spines per 10-μm dendrite length, ANOVA on ranks with Dunn's post hoc).

Thin-shaped dendritic spine densities exhibited similar changes upon treatment with romadepsin (Figure 8(b)). Treatment of burn-injured animals with romidepsin significantly decreased thin-shaped dendritic spine density as compared with DMSO-treated animals (D6: $p < 0.05$, 2.4 ± 0.3 vs. 2.9 ± 0.7 thin spines per 10-μm dendrite length, ANOVA on ranks with Dunn's post

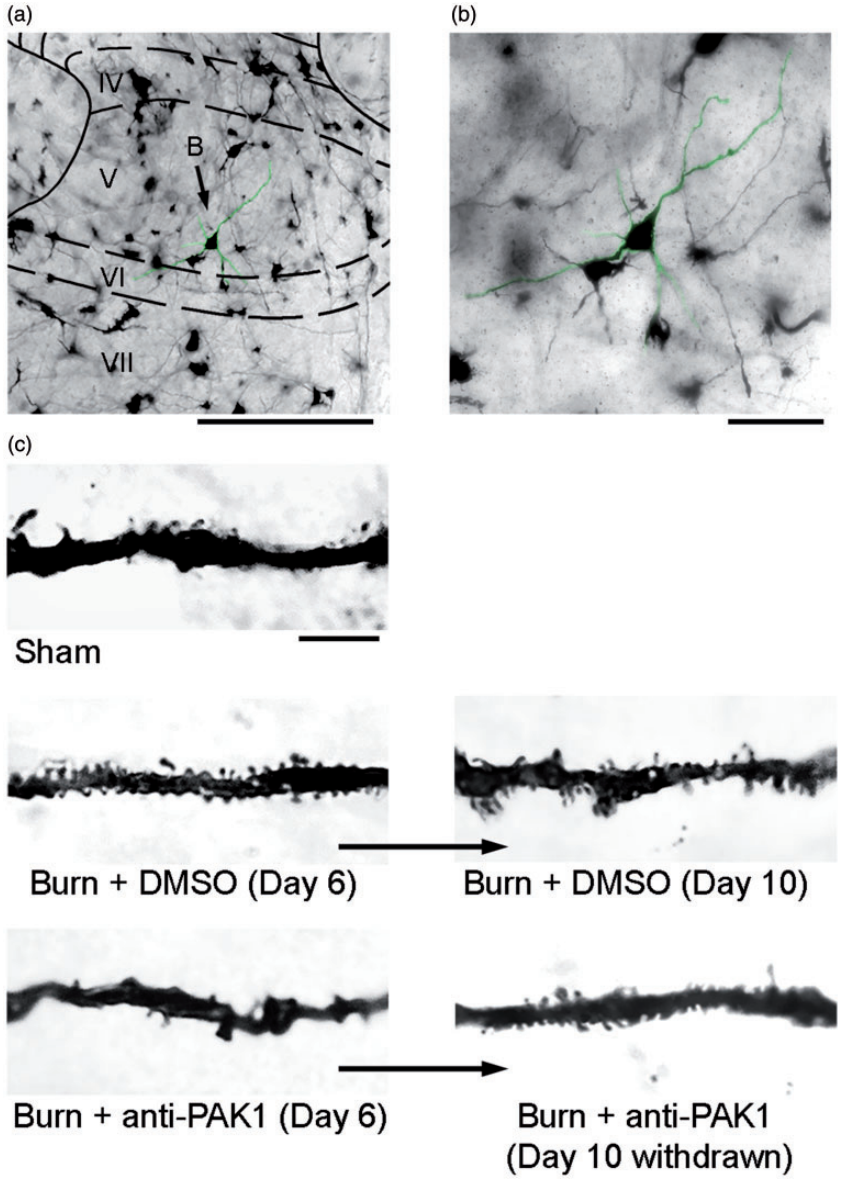

Figure 6. Dendritic spine profiles in the dorsal horn change with burn injury. (a) A representative image of a Golgi-stained coronal section of the dorsal horn with a WDR neuron located within lamina V (green highlight). (b) A high-power field from panel A shows a sample neuron with dendritic branches that extend several hundred microns within the section plane. (c) Neuronal dendritic branches have dendritic spines of various morphology and densities, depending on the treatment condition, for example, burn, drug administered. There are notable qualitative differences in dendritic spine profiles between Sham and burn-injured animal groups, with or without anti-Pak1 romidepsin treatment, and across the experimental time course. Scale bar for (a) is 500 μm, (b) is 100 μm, and (c) is 10 μm. DMSO: dimethyl sulfoxide.

hoc); however, both burn-injured groups had significantly increased thin-shaped spine densities as compared with Sham ($p < 0.05$, 2.1 ± 0.4 thin spines per 10-μm dendrite length). By Day 10, after drug withdrawal, both burn-injured animal groups treated with romidepsin or DMSO continued to have significantly increased thin-shaped dendritic spine densities as compared with Sham (D10: $p < 0.05$, 2.5 ± 0.4 or 2.6 ± 0.9 vs. 2.1 ± 0.4 thin spines per 10-μm dendrite length, ANOVA on ranks with Dunn's post hoc).

Mushroom-shaped dendritic spine density also increased following burn injury in either group treated with romidepsin or DMSO at Day 6 post-burn, as compared with Sham (D6: $p < 0.05$, 0.43 ± 0.2 or 0.58 ± 0.2 vs. 2.8 ± 0.4 mushroom spines per 10-μm dendrite length, one-way ANOVA with Bonferroni's post hoc) (Figure 8(c)). Notably, mushroom-shaped spine density in burn-injured animals treated with DMSO control increased by more than 100% compared to Sham with no burn (from 2.8 to 5.8 mushroom spines per 10-μm

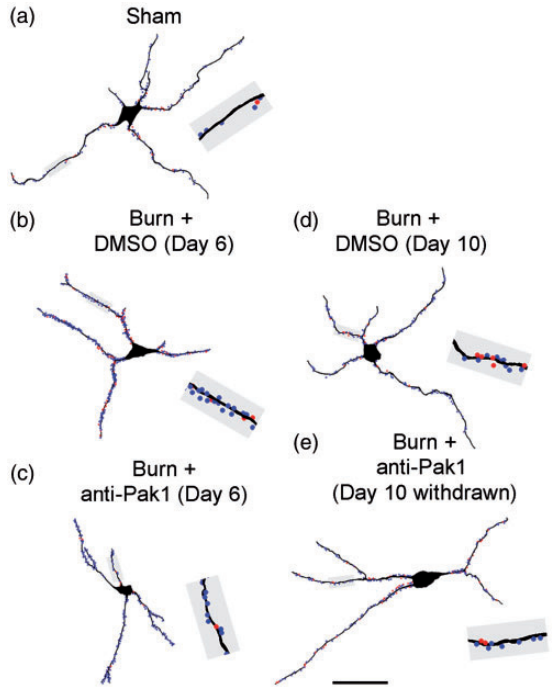

Figure 7. Reconstruction of sampled dorsal horn sensory neurons. To analyze and profile dendritic spines, we digitally reconstructed sampled dorsal horn neurons. We performed density and distribution measurements from these reconstructions from each treatment group: (a) Sham, (b) Burn + DMSO (Day 6), (c) Burn + anti-Pak1 (Day 6), (d) Burn + DMSO (Day 10), and (e) Burn + anti-Pak1 (Day 10 withdrawn). An equivalent length of dendritic branch from each neuron in panels (a) to (e) (gray region) show thin-shaped (blue dots) and mushroom-shaped (red dots) dendritic spines. Scale bar is 50 μm. DMSO: dimethyl sulfoxide.

dendrite). Romidepsin treatment significantly decreased mushroom-spine densities in animals treated with DMSO (D6: $p < 0.05$, 0.43 ± 0.2 vs. 0.58 ± 0.2 mushroom spines per 10-μm dendrite length). At Day 10, romidepsin and DMSO-treated burn-injured animals continued to have significantly increased mushroom-shaped spine density as compared with Sham (D10: $p < 0.05$, 0.47 ± 0.2 or 0.48 ± 0.3 vs. 0.28 ± 0.4 mushroom spines per 10-μm dendrite length). The effect of romidepsin treatment appeared transient, since drug discontinuation resulted in mushroom-dendritic spine densities that were similar to control burn-injured animals treated with DMSO ($p > 0.05$).

Dendritic spines redistribute on dendritic branches after burn injury

The proximity of dendritic spines relative to the cell body can have a significant impact on postsynaptic excitability, that is, synaptic inputs located closer to the axon hillock improves transmission output.[37,48,49] To profile dendritic spine distribution, we applied a Sholl's analysis on reconstructed neuronal samples (Figure 9). At Day 6 after burn injury, total spine density increased along proximal dendrites of sampled neurons in burn-injured animals treated with DMSO as compared with Sham (D6: $\#p < 0.05$; 50 μm: 4.6 ± 2.4 vs. 3.4 ± 0.6; 100 μm: 3.7 ± 1.0 vs. 1.9 ± 0.7; 150 μm: 3.5 ± 1.2 vs. 2.4 ± 0.2; 200 μm: 3.1 ± 1.3 vs. 1.7 ± 0.6; 300 μm: 3.2 ± 2.2 vs. 1.4 ± 0.1; 350 μm: 2.5 ± 0.9 vs. 1.2 ± 0.1 total spines/10 μm dendrite; ANOVA on ranks with Dunn's post hoc) (Figure 9(a)). Treatment with romidepsin in burn-injured animals significantly decreased total dendritic spine density in these regions closest to the cell body as compared with DMSO-treated burn-injured animals ($*p < 0.05$; 50 μm: 3.2 ± 1.2 vs. 4.6 ± 2.4; 100 μm: 2.9 ± 1.2 vs. 3.7 ± 1.0; 150 μm: 2.8 ± 1.0 vs. 3.5 ± 1.2 total spines/10 μm dendrite; ANOVA on ranks with Dunn's post hoc). At this time point, there was no significant difference in total dendritic spine density between romidepsin-treated burn-injured animals and Sham at any dendritic region ($p > 0.05$).

Thin-shaped dendritic spines also demonstrated similar changes in density along dendritic branch lengths. At Day 6, burn-injured animals treated with DMSO showed increased thin-shaped spine density as compared with Sham (D6: $\#p < 0.05$; 50 μm: 3.6 ± 1.9 vs. 2.8 ± 0.5; 100 μm: 3.1 ± 0.9 vs. 1.7 ± 0.7; 200 μm: 2.6 ± 1.4 vs. 1.5 ± 0.5; 300 μm: 2.8 ± 1.9 vs. 1.3 ± 0.2 thin spines/10 μm dendrite; ANOVA on ranks with Dunn's post hoc) (Figure 9(b)). Romidepsin treatment significantly reduced thin-shaped dendritic spine density in the closest three regions to the cell body following burn injury, as compared with burn-injured animals treated with DMSO ($*p < 0.05$; 50 μm: 2.6 ± 0.9 vs. 3.6 ± 1.9; 100 μm: 2.5 ± 0.9 vs. 3.1 ± 0.9; and 150 μm: 2.3 ± 0.9 vs. 3.0 ± 1.2 thin spines/10 μm dendrite; ANOVA on ranks with Dunn's post hoc). Moreover, romidepsin treatment of burn-injured animals resulted in thin-shaped dendritic spine densities that were similar to Sham at all dendrite regions ($p > 0.05$).

In analyses of mushroom-shaped spines, density significantly increased in proximal dendrite regions as compared with Sham; notably with a nearly 100% increase in the 50-μm dendritic length region (D6: $\#p < 0.05$; 50 μm: 1.1 ± 0.8 vs. 0.6 ± 0.2; 100 μm: 0.6 ± 0.3 vs. 0.3 ± 0.1; 150 μm: 0.5 ± 0.2 vs. 2.2 ± 0.2; 200 μm: 0.4 ± 0.3 vs. 0.2 ± 0.2 mushroom spines/10 μm dendrite; ANOVA on ranks with Dunn's post hoc) (Figure 9(c)). As compared with DMSO-treated burn-injured animals, romidepsin treatment resulted in a significant decrease in mushroom-shaped dendritic spine density at the closest region, 50 μm ($*p < 0.05$; 50 μm: 0.6 ± 0.4 vs. 1.1 ± 0.8 mushroom spines/10 μm dendrite; ANOVA on ranks with Dunn's post hoc). There were no significant differences in mushroom dendritic spine

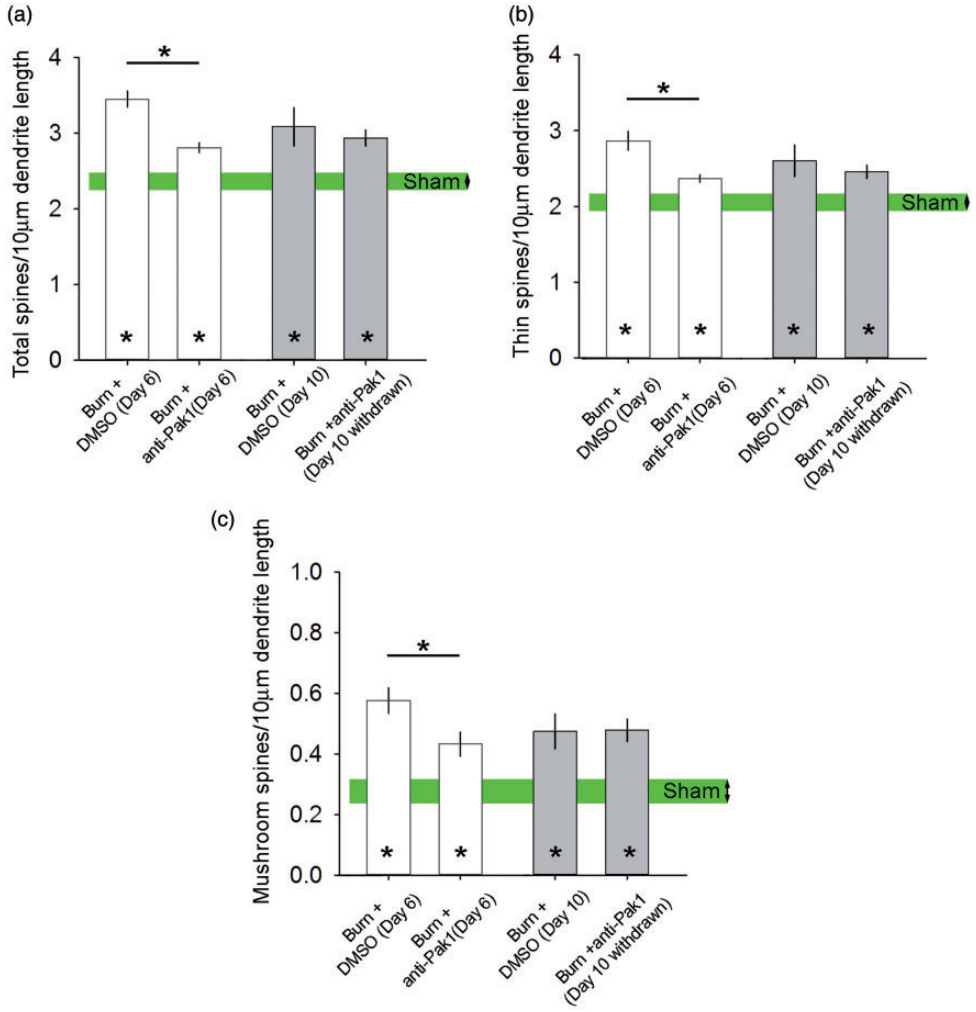

Figure 8. Dendritic spine density. All burn-injured animals treated with DMSO or romidepsin had significantly increased (a) total dendritic spine density, (b) thin-shaped spine density, and (c) mushroom-shaped spine density as compared with Sham on Day 6 or Day 10 (*$p < 0.05$). Assessment of dendritic spine density on Day 6 within 24 h of last drug dosing demonstrated that romidepsin treatment significantly reduced dendritic spine density as compared with DMSO treatment (*$p < 0.05$). By Day 10 after drug treatment withdrawal, there was no detectable difference between these burn-injured treatment groups ($p > 0.05$). Graphs are mean ± SEM. DMSO: dimethyl sulfoxide.

density between romidepsin-treated burn-injured animals and Sham at any region ($p > 0.05$). Taken together, these results demonstrate that romidepsin treatment can reduce dendritic spine density along dendrite regions nearest the cell body following burn injury to levels that are close-to-normal (e.g., no difference with Sham).

After drug withdrawal at Day 10, DMSO-treated animals with burn injury continued to have increased total and thin-shaped dendritic spine density as compared with Sham at the 100-μm dendrite length region (D10: #$p < 0.05$; 100 μm: 2.9 ± 1.1 vs. 1.9 ± 0.7 total spines/10 μm dendrite, or 2.5 ± 0.9 vs. 1.7 ± 0.7 thin spines/10 μm dendrite; ANOVA on ranks with Dunn's post hoc) (Figure 9(d) and (e)). There was no significant difference between romidepsin-treated burn-injured animals as compared with either Sham or DMSO-treated burn-injured animals in any dendritic length region from the cell body ($p > 0.05$). In burn-injured animals treated with romidepsin, mushroom-shaped dendritic spine density was significantly less in a single dendrite region, 100 μm, as compared with DMSO-treated burn-injured animals (D10: *$p < 0.05$; 100 μm: 0.4 ± 0.2 vs. 0.8 ± 0.4 mushroom spines/10 μm dendrite, ANOVA on ranks with Dunn's post hoc) (Figure 9(f)). In this same region, burn-injured animals with DMSO treatment had significantly increased mushroom-shaped dendritic spines as compared with Sham (#$p < 0.05$; 100 μm: 0.8 ± 0.4 vs. 0.3 ± 0.1 mushroom spines/10 μm dendrite, ANOVA on ranks with Dunn's post hoc). There was

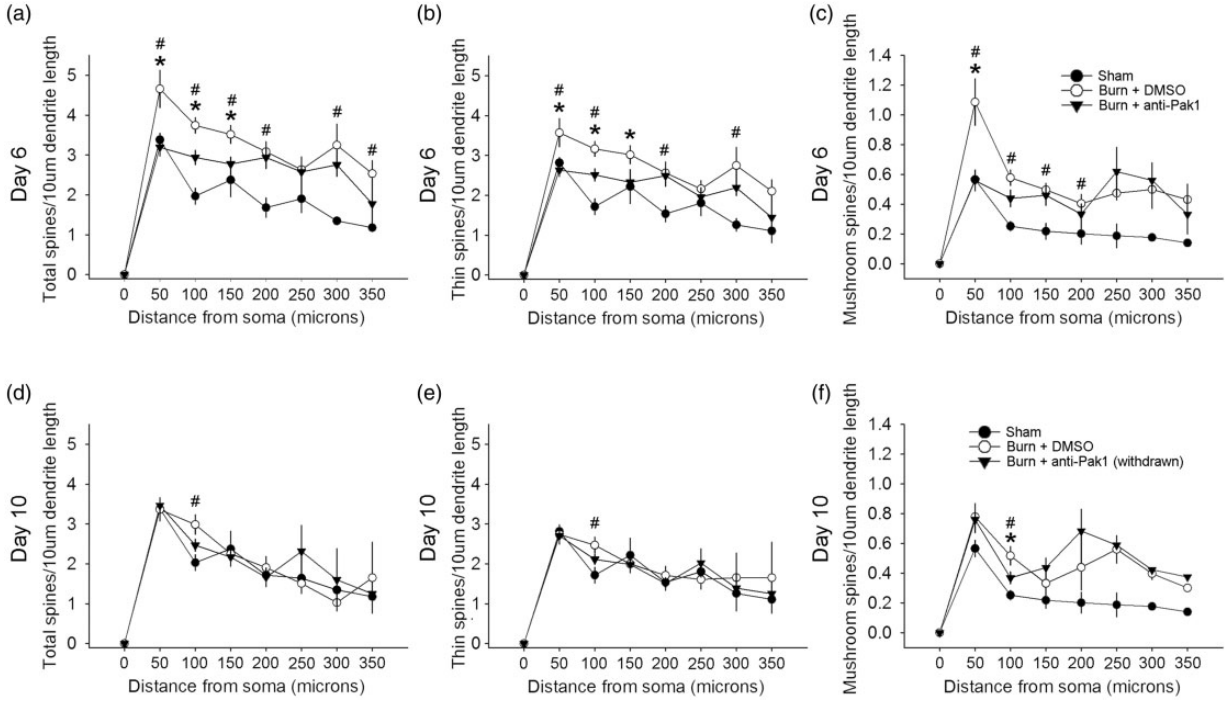

Figure 9. Dendritic spine distribution. To profile dendritic spine distribution, we performed a Sholl's analysis. At Day 6, an analysis of the distribution of (a) total dendritic spine, (b) thin-shaped spines, and (c) mushroom-shaped spines showed preferential increases in density within the dendrite regions closest to the cell body after burn injury + DMSO treatment, as compared with Sham (#$p < 0.05$). In burn-injured animals treated with romidepsin, we observed a significant decrease in density in multiple dendrite regions from the cell body as compared with DMSO-treated burn-injured animals (*$p < 0.05$). We observed no differences between romidepsin-treated burn-injured animals and Sham dendritic spine profiles ($p > 0.05$). At Day 10 following withdrawal of drug treatments, the density of (d) total spines, (e), thin-shaped spines, and (f) mushroom-shaped spines remained significantly greater in burn-injured animals treated with DMSO than compared with Sham at the 100 μm region (#$p < 0.05$). Following romidepsin withdrawal in burn-injured animals, (e) mushroom-shaped dendritic spine density was significantly less than control, DMSO-treated burn-injured animals at the 100 μm region (*$p < 0.05$). For any spine-shape classification, at the Day 10 time point, we observed no significant difference between burn-injured animals previously treated with romidepsin and Sham ($p > 0.05$). Graphs are mean ± SEM. DMSO: dimethyl sulfoxide.

no difference in mushroom spine densities between burn-injured animals that had received romidepsin treatment that was withdrawn, as compared with Sham ($p > 0.05$).

Romidepsin attenuates neuropathic pain after burn injury

To determine whether treatment with romidepsin can attenuate neuropathic pain, we performed heat and mechanical pain threshold testing (Figure 10). In heat hyperalgesia testing, we observed a significant decrease in hind paw withdrawal threshold latency (more pain) in both burn-injured animal groups that persisted throughout the experimental period (up to Day 10 post-burn), as compared with baseline (group mean comparison, $p < 0.05$; mean baseline vs. Day 3–10 range: 14.5–15.2 vs. 4.2–8.1 s, ANOVA on ranks) (Figure 10(a)). After burn injury, but prior to romidepsin treatment, both injured groups demonstrated similar heat pain withdrawal thresholds ($p > 0.05$; romidepsin vs DMSO, D3: 5.4 ± 2.1 vs. 5.7 ± 2.3 s). However, during the three-day treatment of romidepsin in burn-injured animals, heat pain threshold significantly increased as compared with DMSO-treated animals ($p < 0.05$; D4: 7.2 ± 4.9 vs. 4.3 ± 1.5 s; D5: 5.9 ± 2.2 vs. 4.2 ± 0.8 s; D6: 6.5 ± 2.8 vs. 4.7 ± 2.1 s; one-way ANOVA). After drug withdrawal (Day 7 and Day 10 post-burn), romidepsin and DMSO-treated burn-injured animals showed no difference in heat pain withdrawal ($p > 0.05$; D7: 5.6 ± 1.5 vs. 5.8 ± 2.6 s; D10: 8.1 ± 2.2 vs. 7.0 ± 1.8 s). In a group mean comparison of burn-injured animal groups, we observed a significant decrease in heat pain threshold following DMSO as compared with before any treatment ($p < 0.05$; D3 group mean vs. DMSO D4–D6: 5.6 ± 2.2 vs. 4.3 ± 1.5 s; ANOVA on ranks) or romidepsin treatment of burn-injured animals ($p < 0.05$; D3 group mean vs. romidepsin D4–D6: 5.6 ± 2.2 vs. 6.6 ± 3.6 s; ANOVA on ranks) (Figure 10(c)). Group mean comparisons also demonstrated that romidepsin treatment significantly increased heat pain withdrawal threshold latency as

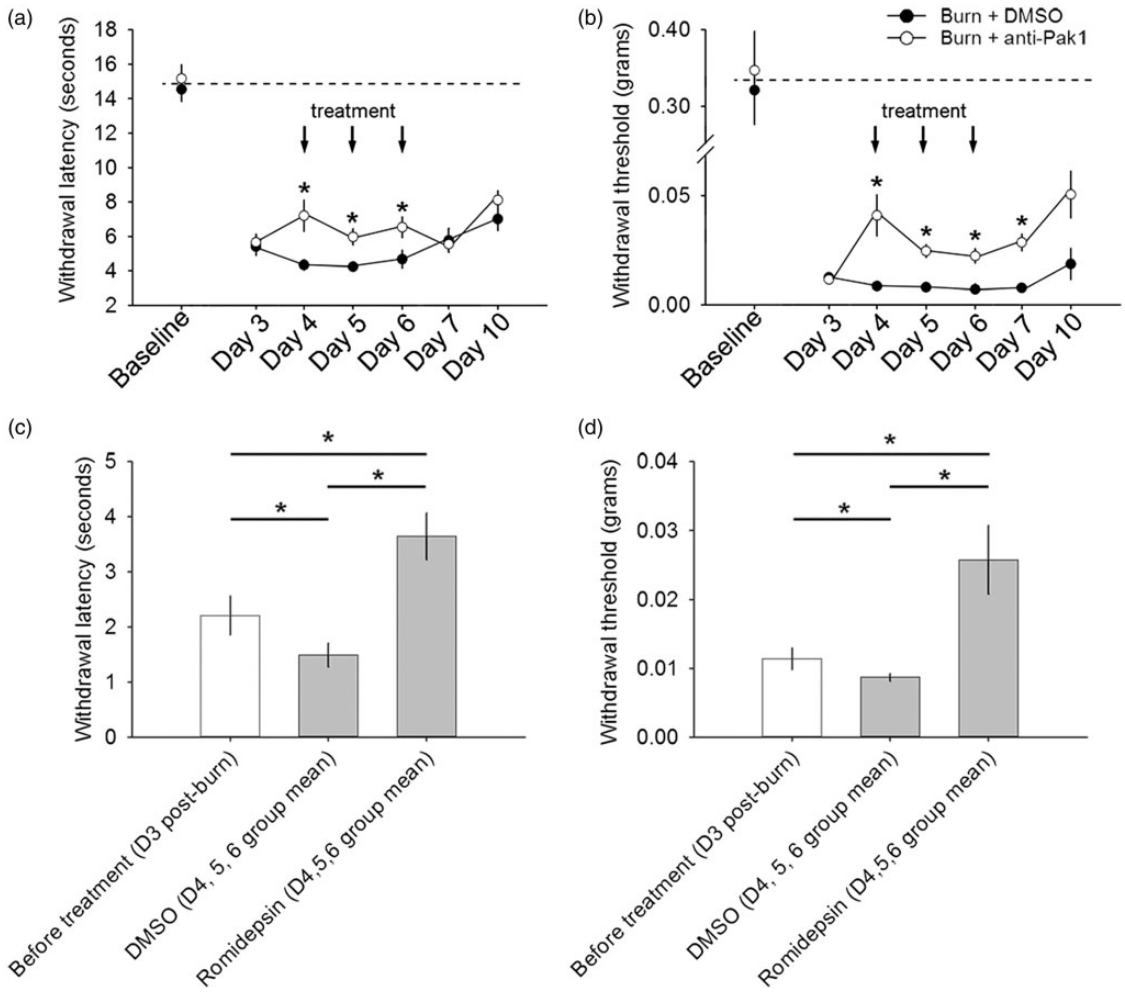

Figure 10. Romidepsin treatment attenuates pain after burn injury. All animals had significantly decreased (a, c) heat and (b, d) mechanical pain thresholds following burn injury. (a) In heat hyperalgesia testing, we observed a decrease in hind paw withdrawal threshold in both burn-injured groups that persisted throughout the experimental period as compared with baseline ($p < 0.05$). During the three-day treatment course with romidepsin, burn-injured animals had a partial but significantly increased heat withdrawal threshold as compared with burned animals treated with DMSO (*$p < 0.05$). Following treatment withdrawal (assessments on Day 7 and Day 10), we observed no differences in heat withdrawal thresholds between burn-injured animal groups ($p > 0.05$). (c) Similarly, in post-burn injury, only comparisons of heat withdrawal threshold, we observed a significant increase in heat withdrawal threshold group mean (i.e., during the treatment period) with romidepsin treatment, as compared with before any treatment (Day 3) or DMSO group mean threshold (*$p < 0.05$). During the DMSO treatment period, we observed a decrease in heat withdrawal threshold as compared with heat withdrawal thresholds before any treatment (*$p < 0.05$). (b) In mechanical pain threshold testing, we observed a decrease in withdrawal threshold that remained throughout the experimental period following burn injury, as compared with baseline ($p < 0.05$). During the three-day treatment with romidepsin, withdrawal thresholds increased as compared with burn-injured animals treated with DMSO (*$p < 0.05$). In burn-injured animals treated with romidepsin, mechanical pain threshold testing on Day 7 demonstrated that increased withdrawal threshold persisted for at least 24 h after romidepsin withdrawal, as compared with burned animals treated with DMSO (*$p < 0.05$). By Day 10, there was no significant difference with mechanical pain thresholds between both burn-injured animal groups ($p > 0.05$). (d) In comparisons of mechanical pain thresholds after burn injury, we observed a significant increase in mechanical withdrawal threshold group mean during romidepsin treatment, as compared with threshold before any treatment or during DMSO treatment (group mean) (*$p < 0.05$). DMSO treatment group mean threshold was significantly less than mechanical pain withdrawal thresholds in burn-injured animals before any treatment (*$p < 0.05$). Graphs are mean ± SEM. DMSO: dimethyl sulfoxide.

compared with DMSO-treated animals ($p < 0.05$; group mean D4–D6, romidepsin vs. DMSO: 6.6 ± 3.6 vs. 4.3 ± 1.5 s; ANOVA on ranks).

In mechanical allodynia testing using systematic application of graded Von Frey filaments, we observed a decrease with tactile pain withdrawal threshold in both burn-injured groups that remained significant until experimental endpoint at Day 10 post-burn, as compared with baseline (group mean comparison, $p < 0.05$; mean baseline vs. Day 3–10 range: 0.32–0.35 vs.

0.01–0.05 g, ANOVA on ranks) (Figure 10(b)). After burn injury, and before romidepsin treatment, both burn-injured groups demonstrated similar tactile pain threshold ($p > 0.05$; romidepsin vs. DMSO, D3: 0.01 $\pm$ 0.001 vs. 0.01 $\pm$ 0.01 g). Over the course of drug treatment, between Day 4 and Day 6, romidepsin treatment increased tactile pain thresholds as compared with DMSO-treated burn-injured animals ($p < 0.05$; D4: 0.04 $\pm$ 0.06 vs. 0.01 $\pm$ 0.009 g; D5: 0.02 $\pm$ 0.02 vs. 0.01 $\pm$ 0.006 g; D6: 0.02 $\pm$ 0.02 vs. 0.009 $\pm$ 0.004 g, ANOVA on ranks). Approximately 24 h after drug withdrawal, romidepsin-treated animals continued to have significantly increased pain threshold as compared with burn-injured animals treated with DMSO ($p < 0.05$; D7: 0.02 $\pm$ 0.01 vs. 0.01 $\pm$ 0.005 g, ANOVA on ranks). This finding suggests that in contrast to heat pain, which rapidly returned to untreated levels within 24 h after drug cessation, romidepsin has a slightly prolonged attenuating effect on tactile pain threshold. By Day 10, however, there was no difference between animals that had been treated with either romidepsin or DMSO ($p > 0.05$; D10: 0.05 $\pm$ 0.05 vs. 0.02 $\pm$ 0.03 g). In a group mean longitudinal comparisons (Figure 10(d)), we observed a significant decrease in tactile pain threshold with DMSO treatment as compared with threshold before any treatment ($p < 0.05$; D3 group mean vs. DMSO D4–D6: 0.01 $\pm$ 0.01 vs. 0.009 $\pm$ 0.004 g; ANOVA on ranks), or after romidepsin treatment ($p < 0.05$; D3 group mean vs. romidepsin D4–D6: 0.01 $\pm$ 01 vs. 0.03 $\pm$ 0.04 g; ANOVA on ranks). Group mean comparisons also demonstrated that romidepsin treatment significantly increased tactile pain threshold as compared with DMSO-treated animals ($p < 0.05$; group mean D4–D6, romidepsin vs. DMSO: 0.03 $\pm$ 0.04 vs. 0.009 $\pm$ 0.004 g; ANOVA on ranks).

Romidepsin does not affect inflammation within the spinal cord after burn injury

We and others have previously shown that spinal cord inflammation occurs after burn injury, and that injury-induced inflammation contributes to maintaining central sensitization and neuropathic pain.[8,50–52] To assess inflammation/gliosis in cutaneous burn injury with or without romidepsin treatment, we analyzed the presence of astrogliosis and microgliosis within the ipsilateral dorsal horn (i.e., burn-injured side) (Figure 11). As shown in Figure 11(a), GFAP immunoreactivity levels appeared to increase following burn injury in animals treated with either DMSO or romidepsin. At Day 6, GFAP expression remained elevated in both burn-injured groups (D6: $p < 0.05$, DMSO or romidepsin vs.

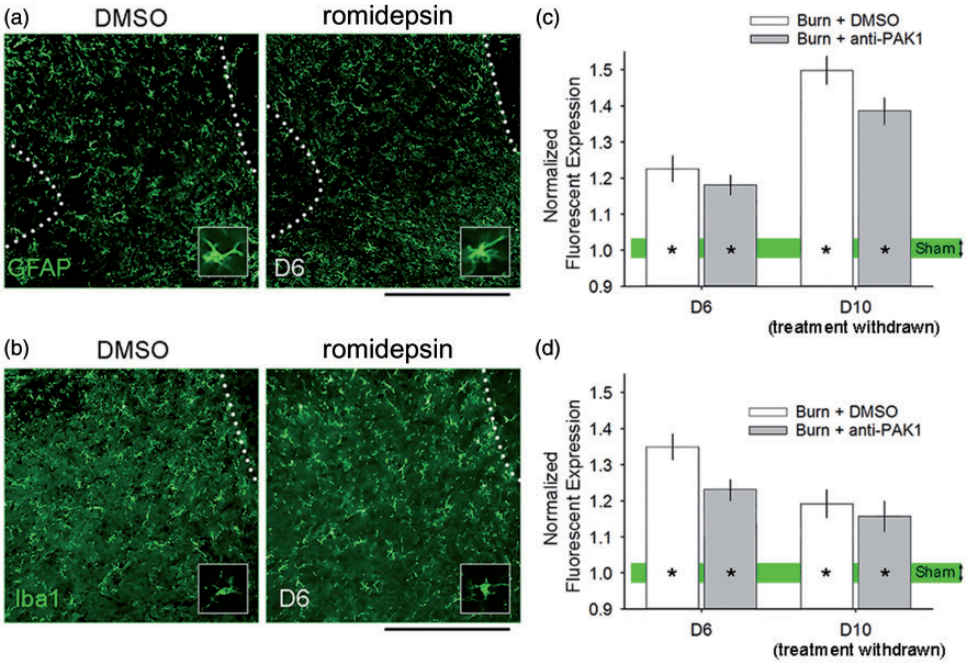

Figure 11. Burn injury-induced inflammation in the spinal cord. At Day 6, all burn-injured animals exhibited increased (a) astrogliosis and (b) microgliosis in the ipsilateral dorsal horn. (c) Expression of GFAP immunoreactivity in burn-injured animals was significantly increased in burn-injured animals with DMSO or romidepsin treatment at Day 6 and Day 10, as compared with Sham (*$p < 0.05$). There was no significant difference in comparisons between burn-injured animals with either drug treatment at either experimental time point ($p > 0.05$). Similarly, (d) expression of Iba1 immunoreactivity in both burn-injured groups was significantly greater within the dorsal horn following DMSO or romidepsin treatment at Day 6 and Day 10, as compared with Sham (*$p < 0.05$). There was no difference between either burn-injured treatment group at either time point ($p > 0.05$). Graphs are mean $\pm$ SEM. DMSO: dimethyl sulfoxide.

Sham: 1.2 ± 0.3 or 1.1 ± 0.2 vs. 1.0 ± 0.1 normalized expression, one-way ANOVA with Bonferroni's post hoc) (Figure 11(c)). There were no significant differences in comparisons between DMSO and romidepsin-treated burn-injured animals ($p > 0.05$). At Day 10, both DMSO and romidepsin-treated animals with burn injury had significantly increased GFAP expression levels, as compared with Sham (D10: $p < 0.05$, DMSO or romidepsin vs. Sham: 1.5 ± 0.2 or 1.4 ± 0.2 vs. 1.0 ± 0.1 normalized expression, one-way ANOVA with Bonferroni's post hoc). Additionally, there was significant difference between DMSO or romidepsin-treated animals with burn injury at Day 10 following treatment discontinuation ($p > 0.05$). In analyses for iba1 expression in the dorsal horn, we observed similar outcomes following burn injury. At Day 6, both DMSO and romidepsin-treated burn-injured animal groups had significantly increased iba1 expression as compared with Sham (D6: $p < 0.05$, DMSO or romidepsin vs. Sham: 1.4 ± 0.2 or 1.2 ± 0.1 vs. 1.0 ± 0.05 normalized expression, one-way ANOVA with Bonferroni's post hoc) (Figure 11(d)). At Day 10 following treatment withdrawal, burn-injured animals with DMSO or romidepsin treatment continued to have significantly increased iba1 expression as compared with Sham (D10: $p < 0.05$, DMSO or romidepsin vs. Sham: 1.2 ± 0.1 or 1.2 ± 0.1 vs. 1.0 ± 0.1 normalized expression, one-way ANOVA with Bonferroni's post hoc). No differences were observed between treated animal groups with burn injury at Day 6 or Day 10 ($p > 0.05$). Interestingly, our observations are consistent with previous work demonstrating that astrocytes and microglia have different time courses for reaching maximal activation after peripheral nerve or burn injuries: microgliosis peaks earlier than astrogliosis, which has a delayed and prolonged presence after injury.[8,53] Taken together, our results demonstrate that our treatment paradigm with romidepsin does not appear to significantly affect the magnitude or time course of burn injury-induced central inflammation within the spinal cord dorsal horn.

Pak1 and Rac1 protein levels show no apparent change following burn injury

Romidepsin can significantly reduce Pak1 activity without changing Pak1 protein level.[54–56] To assess whether romidepsin affects expression of Pak1 or Rac1, we analyzed spinal cord tissue co-labeled with neuronal marker, NeuN (Figure 12). At Day 6, after the last administered dose of DMSO or romidepsin, Pak1 levels in labeled neurons was not significantly different as compared with Sham ($p > 0.05$, DMSO vs. romidepsin vs. Sham; 1.04 ± 0.2 vs. 1.07 ± 0.2 vs. 1.0 ± 0.2 normalized co-

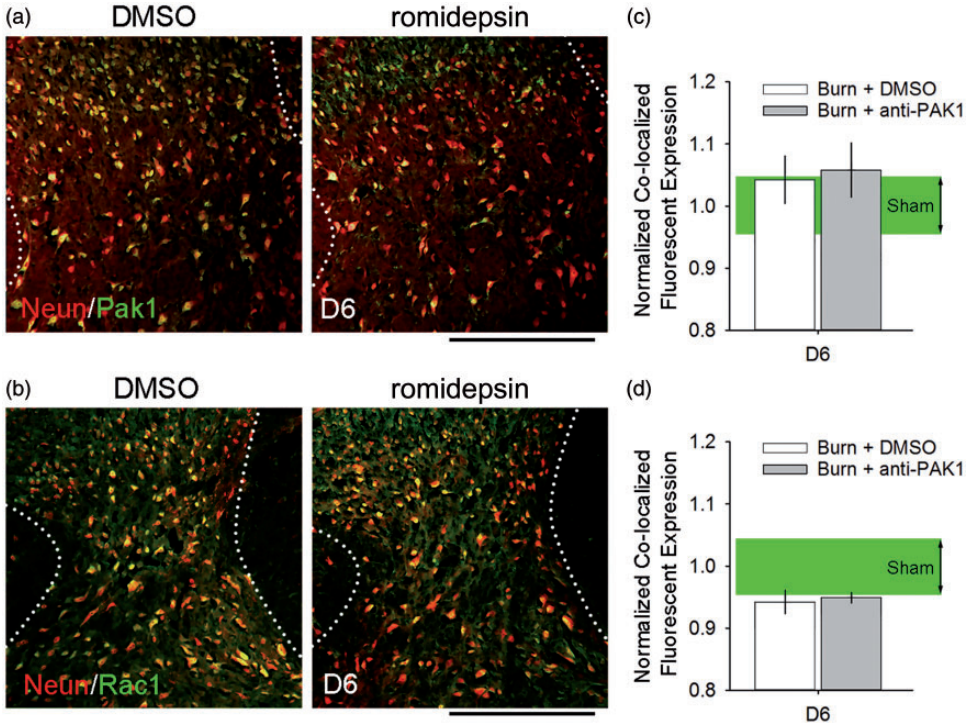

Figure 12. Pak1 and Rac1 expression remain normal after burn injury. All burn-injured animals had similar expression levels of (a, c) Pak1 and (b, d) Rac1 in dorsal horn neurons (co-localized with NeuN immunostaining). At Day 6, there was no significant difference in co-localized (c) Pak1 expression or (d) Rac1 expression between any burn-injured group treated with DMSO or romidepsin and Sham ($p > 0.05$). Graphs are mean ± SEM. DMSO: dimethyl sulfoxide.

localized expression, ANOVA on ranks with Dunn's post hoc) (Figure 12(c)). Similarly, we observed no significant difference in Rac1 expression in neurons ($p > 0.05$, DMSO vs. romidepsin vs. Sham; 0.94 ± 0.1 vs. 0.95 ± 0.05 vs. 1.0 ± 0.2 normalized co-localized expression, ANOVA on ranks with Dunn's post hoc) (Figure 12(b) and Figure 12(d)). Notably, in either outcome, burn injury did not appear to significantly affect expression levels of Rac1 or Pak1 when directly compared with Sham ($p > 0.05$). Taken together, these results are consistent with previous work demonstrating that romidepsin action is due to decreasing Pak1 activity, rather than changes in protein expression.[55,56]

Discussion

Burn injury is a global unmet medical need, affecting millions of individuals, of which a high proportion experience clinically significant pain. Unfortunately, treatment strategies for neuropathic pain are often refractory or short-lived. The failure to satisfactorily address this unmet medical need is due in part to the lack of mechanistic insight into molecular factors underlying neuropathic pain. To address this gap, we leveraged our previous mechanistic studies to identify and assess the potentially novel role of the Pak1 pathway in pain.[11,13,14] Additionally, we tested the feasibility of "repurposing" romidepsin, an existing clinically available drug that targets Pak1 activity, to alleviate burn injury-induced neuropathic pain.

Over the past decade, we have demonstrated the necessary and sufficient contribution of Rac1 signaling in hyperexcitability disorders, including multiple forms of neuropathic pain.[11,13,14,30,57] Importantly, we have shown that Rac1-regulated dendritic spine remodeling in the dorsal horn contributes to neuropathic pain after trauma to the nervous system, including diabetes mellitus, peripheral nerve injury, spinal cord injury, and cutaneous burn injury.[14,24,58,59] In these studies, attenuation of neuropathic pain was achieved when near-normal dendritic spine profiles were successfully restored using a Rac1-inhibitor. Treatment discontinuation resulted in a relapse of both neuropathic pain and abnormal dendritic spine profiles. A caveat of these studies, however, was the low clinical utility of directly targeting Rac1, which has been considered a poor therapeutic target due to its broad intracellular actions.[17] Thus, to advance our goal of addressing burn injury-induced pain, we sought a mechanism-based approach to identify an alternative and clinically relevant molecular target for addressing neuropathic pain.

Based on our published work and others,[11,19,20,60] we hypothesized that pharmacological inhibition of Pak1 would be a druggable target for the treatment of neuropathic pain. Pak1 is a downstream effector of Rac1 that links Rac1 activity to cytoskeletal actin reorganization involved in dendritic spine remodeling.[61] Importantly, Pak1 is an already established clinical target for cancer and neurological disease but has not been investigated for addressing chronic pain conditions.[19,43] To test our hypothesis, we identified the clinically approved Pak1-inhibitor, romidepsin, approved by the US FDA in 2009 for the treatment of lymphoma.[44] Romidepsin is a potent HDAC inhibitor that reduces Pak1 activity without affecting its protein level. As shown in pharmacokinetic/pharmacodynamic (PK/PD) studies in rodent and non-human primates, romidepsin's active metabolites are bioavailable to the CNS, passively penetrating the BBB following systemic administration.[62] In our present study, we performed a dose–response assessment to identify the MTD at which we observed an analgesic effect without significant adverse effect to body weight, mobility/strength, and affective-cognitive exploratory behavior. In our burn injury model, we further confirmed that systemic administration via an i.p. route resulted in the positive expression of two established drug response biomarkers in the spinal cord dorsal horn, that is, increased histone acetylation and decreased p-Raf (a downstream effector of Pak1).[45,46,62]

To examine the contribution of Pak1 activity in neuropathic pain following burn injury, we assessed the efficacy of romidepsin in reducing cellular and structural pain correlates and burn injury-induced neuropathic pain. Treatment with romidepsin significantly reduced cellular correlates of pain (see summary in Table 2). Within 24 h of drug treatment, we observed a significant reduction in c-fos expression (e.g., a marker for neuronal activity), attenuated dendritic spine dysgenesis in the dorsal horn, and a partial, but significant restoration of pain threshold. After treatment withdrawal, however, all outcome assessments returned to untreated, burn-injured animal levels. Importantly, we found no effect of romidepsin treatment on the inflammatory response in the spinal cord at any time point. Collectively, our results show for the first time that Pak1 activity contributes to neuropathic pain.

An important mechanistic question, partially addressed in this study, focuses on how a second-degree burn injury can lead to chronic, long-lasting pain with neuropathic symptoms. Although superficial, burn injuries are multifaceted insults to neuronal and non-neuronal tissues. Damaged skin and injured intracutaneous nerves release chemokines, trophic factors, and inflammatory mediators, for example, tumor necrosis factor-alpha or matrix metalloproteinase-9, which can contribute to inflammation at the site of burn injury, as part of the healing process, as well as remotely through long-distance signaling.[63–68] Scar tissue formation at the site of burn injury can also become sensitized, increasing nerve excitability which may be attributed to

Table 2. Summary findings of treatment comparisons.

Endpoint post-burn	Treatment group	Body weight/ motor control	H3/p-Raf (drug response biomarkers)	c-fos+	Dendritic spine dysgenesis[a]	Pain threshold	Iba1/GFAP	Rac1/Pak1
Day 6	Burn + DMSO	∅	↑	↓	↓*	↑*	*	∅
	Burn + anti-Pak1							
Day 10 (drug withdrawn)	Burn + DMSO		∅	*	*	*		
	Burn + anti-Pak1							
	Sham				Control			

Note: Dendritic spine dysgenesis outcome measures include changes in density and distribution. Pain threshold measures include behavioral assessments for tactile allodynia and heat hyperalgesia. DMSO: dimethyl sulfoxide; ∅: no significant change in any tests; ↑↓: significant up/down change following anti-Pak1 treatment; *: significant difference from Sham control values.

[a]Defined as different from Sham control values.

sodium channel misexpression, for example, Nav1.3.[25,69–71] We show here that burn injury induced central inflammation including the activation of microglia and astrocytes within the ipsilateral dorsal horn. Microglia activate early within the spinal cord, whereas astrocyte activation follows and contributes to maintaining central sensitization, even as maximal levels of microgliosis progressively declines.[8,50,72,73] Astrocyte activation reaches maximal levels by one week after second-degree burn injury in rodents.[8,50] Consistent with these previous observations, we observed a significant inflammatory response related to increased microgliosis and astrogliosis within the ipsilateral dorsal horn after second degree after burn injury.

Pak1 links Rac1 activity to cytoskeletal reorganization through its modulation of actin and microtubule dynamics.[74] Importantly, Pak1 is localized at dendritic spines, interacts with post-synaptic density protein, PSD-95, and f-actin, and may directly mediate dendritic spine formation and long-term maintenance.[74] Dominant-negative Pak1 expression results in fewer dendritic spines, whereas constitutively active Pak1 increases the number of dendritic spines on hippocampal neurons. Taken together, these results strongly suggest that activation of Pak1 is essential for the formation, maturation, and stability of dendritic spines. Notably, Pak1 mutation and dysregulation has been shown to contribute to neurological diseases and disorders, including cognitive defects, mental retardation, and neuropsychiatric diseases.[19–21] Until this report, the role of Pak1 in chronic pain or hyperexcitability disorders in the CNS has not been studied.

Our current results are consistent with previous work demonstrating that dendritic spine dysgenesis in nociceptive sensory neurons in the dorsal horn contributes to both burn injury and peripheral nerve injury-induced neuropathic pain conditions.[14,58] Dendritic spines on WDR neurons change in shape and profile predictably through a common motif strongly associated with pain.[11] Although it is not known how burn injury or any insult to the nervous system triggers dendritic spine remodeling, our previous work has shown that the Rac1-Pak1 molecular pathway regulates dendritic spine remodeling involved in neuropathic pain. Here, we observed altered dendritic spine morphology in the intermediate zone following burn injury, which was accompanied by pain-related behavior (Table 2). Romidepsin treatment in burn-injured animals reduced dendritic spine dysgenesis in the intermediate zone, marked by decreases in dendritic spine density and spatial redistribution that was similar to control, unburned animals. Consistent with this, we also observed c-fos expression increase following burn injury at this time point at Day 6, suggesting that burn injury increases neuronal excitability, as previously reported.[25] Importantly, treatment with romidepsin decreased c-fos expression in a topographically restricted manner, only reducing c-fos expression in the intermediate zone (laminae IV–V). This histological profile of romidepsin treatment in reducing c-fos expression and dendritic spine dysgenesis suggests that the drug's primary action can reduce spinal cord hyperexcitability across a wide-range of sensory modalities (i.e., high- and low-threshold afferent input converge on interneurons located in the intermediate zone). Although our results show no statistically significant effect in other dorsal or ventral laminae of the spinal cord, which we have previously investigated,[8,14] we note the caveat that our measures here may not have had sufficient sensitivity within our sample size to preclude this possibility. Nonetheless, our results demonstrate that romidepsin treatment has a predictable effect upon cellular and structural correlates of pain in the dorsal horn nociceptive-sensory system after burn injury.

A notable caveat to our study is the possibility that spontaneous pain recovery could mask a longer term analgesic effect of romidepsin treatment. We expected that the effectiveness of romidepsin would be limited by its half-life (<10 h) and bioavailability.[43,44] This assumption, however, comes from PK/PD studies performed in other species, which may have different metabolic status

than our mouse model. Although we observed no effect on inflammation in the spinal cord, we cannot rule out the possibility of an effect in the peripheral nervous system which was not studied here. Therefore, it is possible that Pak1 inhibition could influence other factors along the pain axis. Note that we report that romidepsin at MTD did not affect body weight, general mobility, or exploratory-rearing behaviors. Nonetheless, our study raises the need for further investigation on the (1) longer term use of romidepsin or other Pak1 inhibitors, (2) its effect on peripheral tissue, and (3) its efficacy at lower doses if administered centrally, which could improve the drug's bioavailability to nociceptive tissues in the dorsal horn. Irrespective of these caveats, our results raise the possibility that inhibition of Pak1, either by small-molecule inhibitors such as romidepsin, or via gene therapy approaches, may have a role in the treatment of pain following burn injury.

In summary, our findings demonstrate for the first time a role for Pak1 signaling in mechanisms underlying pain. Our findings identify Pak1 signaling as a potential molecular target for therapeutic intervention in traumatic burn-induced neuropathic pain. More generally, this study demonstrates that preclinical studies can be leveraged to identify clinically available drugs, such as romidepsin, that may be repurposed for addressing intractable pain.

Acknowledgment

The authors thank Shujun Liu and Peng Zhao for their excellent technical assistance.

Declaration of Conflicting Interests

The author(s) declared no potential conflicts of interest with respect to the research, authorship, and/or publication of this article.

Funding

The author(s) disclosed receipt of the following financial support for the research, authorship, and/or publication of this article: This work was supported in part by grants from the Medical Research Service and Rehabilitation Research Service, Department of Veterans Affairs. The Center for Neuroscience and Regeneration Research is a Collaboration of the Paralyzed Veterans of America and Yale University. AMT is funded through the generous support of the PVA Research Foundation, Taylor Foundation for Chronic Diseases, and a VA Career Development Award (1-IK2-RX-001123–01-A2). YG was funded in part by the China Scholarship Council.

References

1. Latarjet J and Choinere M. Pain in burn patients. *Burns* 1995; 21: 344–348.
2. Bijlard E, Uiterwaal L, Kouwenberg CA, Mureau MA, Hovius SE and Huygen FJ. A systematic review on the prevalence, etiology, and pathophysiology of intrinsic pain in dermal scar tissue. *Pain Physician* 2017; 20: 1–13.
3. Browne AL, Andrews R, Schug SA and Wood F. Persistent pain outcomes and patient satisfaction with pain management after burn injury. *Clin J Pain* 2011; 27: 136–145.
4. Dauber A, Osgood PF, Breslau AJ, Vernon HL and Carr DB. Chronic persistent pain after severe burns: a survey of 358 burn survivors. *Pain Med* 2002; 3: 6–17.
5. Peck MD. Epidemiology of burns throughout the world. Part I: distribution and risk factors. *Burns* 2011; 37: 1087–1100.
6. Van Loey NE and Van Son MJ. Psychopathology and psychological problems in patients with burn scars: epidemiology and management. *Am J Clin Dermatol* 2003; 4: 245–272.
7. Atchison NE, Osgood PF, Carr DB and Szyfelbein SK. Pain during burn dressing change in children: relationship to burn area, depth and analgesic regimens. *Pain* 1991; 47: 41–45.
8. Chang YW, Tan A, Saab C and Waxman S. Unilateral focal burn injury is followed by long-lasting bilateral allodynia and neuronal hyperexcitability in spinal cord dorsal horn. *J Pain* 2010; 11: 119–130.
9. Fischer TZ and Waxman SG. Extraterritorial temperature pain threshold abnormalities in subjects with healed thermal injury. *J Rehabil Res Dev* 2012; 49: 515–522.
10. Boros BD, Greathouse KM, Gentry EG, Curtis KA, Birchall EL, Gearing M and Herskowitz JH. Dendritic spines provide cognitive resilience against Alzheimer's disease. *Ann Neurol* 2017; 82: 602–614.
11. Zhao P, Hill M, Liu S, Chen L, Bangalore L, Waxman SG and Tan AM. Dendritic spine remodeling following early and late Rac1 inhibition after spinal cord injury: evidence for a pain biomarker. *J Neurophysiol* 2016; 115: 2893–2910.
12. Cao XC, Pappalardo LW, Waxman SG and Tan AM. Dendritic spine dysgenesis in superficial dorsal horn sensory neurons after spinal cord injury. *Mol Pain* 2017; 13: 1744806916688016.
13. Tan AM. Dendritic spine dysgenesis in neuropathic pain. *Prog Mol Biol Transl Sci* 2015; 131: 385–408.
14. Tan AM, Samad OA, Liu S, Bandaru S, Zhao P and Waxman SG. Burn injury-induced mechanical allodynia is maintained by Rac1-regulated dendritic spine dysgenesis. *Exp Neurol* 2013; 248: 509–519.
15. Senger DL, Tudan C, Guiot MC, Mazzoni IE, Molenkamp G, LeBlanc R, Antel J, Olivier A, Snipes GJ and Kaplan DR. Suppression of Rac activity induces apoptosis of human glioma cells but not normal human astrocytes. *Cancer Res* 2002; 62: 2131–2140.
16. Tolias KF, Bikoff JB, Kane CG, Tolias CS, Hu L and Greenberg ME. The Rac1 guanine nucleotide exchange factor Tiam1 mediates EphB receptor-dependent dendritic spine development. *Proc Natl Acad Sci USA* 2007; 104: 7265–7270.
17. Gysin S, Salt M, Young A and McCormick F. Therapeutic strategies for targeting ras proteins. *Genes Cancer* 2011; 2: 359–372.

18. Allen JD, Jaffer ZM, Park SJ, Burgin S, Hofmann C, Sells MA, Chen S, Derr-Yellin E, Michels EG, McDaniel A, Bessler WK, Ingram DA, Atkinson SJ, Travers JB, Chernoff J and Clapp DW. p21-activated kinase regulates mast cell degranulation via effects on calcium mobilization and cytoskeletal dynamics. *Blood* 2009; 113: 2695–2705.
19. Kichina JV, Goc A, Al-Husein B, Somanath PR and Kandel ES. PAK1 as a therapeutic target. *Expert Opin Ther Targets* 2010; 14: 703–725.
20. Ma QL, Yang F, Frautschy SA and Cole GM. PAK in Alzheimer disease, Huntington disease and X-linked mental retardation. *Cell Logist* 2012; 2: 117–125.
21. Nikolic M. The Pak1 kinase: an important regulator of neuronal morphology and function in the developing forebrain. *Mol Neurobiol* 2008; 37: 187–202.
22. Gao Y, Dickerson JB, Guo F, Zheng J and Zheng Y. Rational design and characterization of a Rac GTPase-specific small molecule inhibitor. *Proc Natl Acad Sci USA* 2004; 101: 7618–7623.
23. Shin YJ, Kim EH, Roy A and Kim JH. Evidence for a novel mechanism of the PAK1 interaction with the Rho-GTPases Cdc42 and Rac. *PLoS One* 2013; 8: e71495.
24. Tan AM, Stamboulian S, Chang YW, Zhao P, Hains AB, Waxman SG and Hains BC. Neuropathic pain memory is maintained by Rac1-regulated dendritic spine remodeling after spinal cord injury. *J Neurosci* 2008; 28: 13173–13183.
25. Shields SD, Cheng X, Uceyler N, Sommer C, Dib-Hajj SD and Waxman SG. Sodium channel Na(v)1.7 is essential for lowering heat pain threshold after burn injury. *J Neurosci* 2012; 32: 10819–10832.
26. Deacon RM. Measuring the strength of mice. *J Vis Exp*. Epub ahead of print 2 June 2013. DOI: 10.3791/2610.
27. Chaplan SR, Bach FW, Pogrel JW, Chung JM and Yaksh TL. Quantitative assessment of tactile allodynia in the rat paw. *J Neurosci Methods* 1994; 53: 55–63.
28. Dirig DM, Salami A, Rathbun ML, Ozaki GT and Yaksh TL. Characterization of variables defining hindpaw withdrawal latency evoked by radiant thermal stimuli. *J Neurosci Methods* 1997; 76: 183–191.
29. Shields SD, Ahn HS, Yang Y, Han C, Seal RP, Wood JN, Waxman SG and Dib-Hajj SD. Nav1.8 expression is not restricted to nociceptors in mouse peripheral nervous system. *Pain* 2012; 153: 2017–2030.
30. Bandaru SP, Liu S, Waxman SG and Tan AM. Dendritic spine dysgenesis contributes to hyperreflexia after spinal cord injury. *J Neurophysiol* 2015; 113: 1598–1615.
31. Tan AM, Chakrabarty S, Kimura H and Martin JH. Selective corticospinal tract injury in the rat induces primary afferent fiber sprouting in the spinal cord and hyperreflexia. *J Neurosci* 2012; 32: 12896–12908.
32. Woolf CJ and King AE. Physiology and morphology of multireceptive neurons with C-afferent fiber inputs in the deep dorsal horn of the rat lumbar spinal cord. *J Neurophysiol* 1987; 58: 460–479.
33. Kim BG, Dai HN, McAtee M, Vicini S and Bregman BS. Remodeling of synaptic structures in the motor cortex following spinal cord injury. *Exp Neurol* 2006; 198: 401–415.
34. Bourne J and Harris KM. Do thin spines learn to be mushroom spines that remember? *Curr Opin Neurobiol* 2007; 17: 381–386.
35. Chen LY, Rex CS, Casale MS, Gall CM and Lynch G. Changes in synaptic morphology accompany actin signaling during LTP. *J Neurosci* 2007; 27: 5363–5372.
36. Holmes WR. Is the function of dendritic spines to concentrate calcium? *Brain Res* 1990; 519: 338–342.
37. Tan AM, Choi JS, Waxman SG and Hains BC. Dendritic spine remodeling after spinal cord injury alters neuronal signal processing. *J Neurophysiol* 2009; 102: 2396–2409.
38. Tashiro A and Yuste R. Structure and molecular organization of dendritic spines. *Histol Histopathol* 2003; 18: 617–634.
39. Yuste R, Majewska A and Holthoff K. From form to function: calcium compartmentalization in dendritic spines. *Nat Neurosci* 2000; 3: 653–659.
40. Adams LM and Geyer MA. A proposed animal model for hallucinogens based on LSD's effects on patterns of exploration in rats. *Behav Neurosci* 1985; 99: 881–900.
41. Ahmadi M, Dufour JP, Seifritz E, Mirnajafi-Zadeh J and Saab BJ. The PTZ kindling mouse model of epilepsy exhibits exploratory drive deficits and aberrant activity amongst VTA dopamine neurons in both familiar and novel space. *Behav Brain Res* 2017; 330: 1–7.
42. Sheets AL, Lai PL, Fisher LC and Basso DM. Quantitative evaluation of 3D mouse behaviors and motor function in the open-field after spinal cord injury using markerless motion tracking. *PLoS One* 2013; 8: e74536.
43. Bertino EM and Otterson GA. Romidepsin: a novel histone deacetylase inhibitor for cancer. *Expert Opin Investig Drugs* 2011; 20: 1151–1158.
44. VanderMolen KM, McCulloch W, Pearce CJ and Oberlies NH. Romidepsin (Istodax, NSC 630176, FR901228, FK228, depsipeptide): a natural product recently approved for cutaneous T-cell lymphoma. *J Antibiot* 2011; 64: 525–531.
45. Kalwat MA, Yoder SM, Wang Z and Thurmond DC. A p21-activated kinase (PAK1) signaling cascade coordinately regulates F-actin remodeling and insulin granule exocytosis in pancreatic beta cells. *Biochem Pharmacol* 2013; 85: 808–816.
46. Zang M, Gong J, Luo L, Zhou J, Xiang X, Huang W, Huang Q, Luo X, Olbrot M, Peng Y, Chen C and Luo Z. Characterization of Ser338 phosphorylation for Raf-1 activation. *J Biol Chem* 2008; 283: 31429–31437.
47. Chung L. A brief introduction to the transduction of neural activity into Fos signal. *Dev Reprod* 2015; 19: 61–67.
48. Pongracz F. The function of dendritic spines: a theoretical study. *Neuroscience* 1985; 15: 933–946.
49. Segev I and Rall W. Computational study of an excitable dendritic spine. *J Neurophysiol* 1988; 60: 499–523.
50. Chang YW and Waxman SG. Minocycline attenuates mechanical allodynia and central sensitization following peripheral second-degree burn injury. *J Pain* 2010; 11: 1146–1154.
51. Kerr BJ, Gupta Y, Pope R, Thompson SW, Wynick D and McMahon SB. Endogenous galanin potentiates spinal

nociceptive processing following inflammation. *Pain* 2001; 93: 267–277.
52. Todd AJ. Neuronal circuitry for pain processing in the dorsal horn. *Nat Rev Neurosci* 2010; 11: 823–836.
53. Hains BC and Waxman SG. Activated microglia contribute to the maintenance of chronic pain after spinal cord injury. *J Neurosci* 2006; 26: 4308–4317.
54. Hirokawa Y, Arnold M, Nakajima H, Zalcberg J and Maruta H. Signal therapy of breast cancers by the HDAC inhibitor FK228 that blocks the activation of PAK1 and abrogates the tamoxifen-resistance. *Cancer Biol Ther* 2005; 4: 956–960.
55. Maruta H. Effective neurofibromatosis therapeutics blocking the oncogenic kinase PAK1. *Drug Discov Ther* 2011; 5: 266–278.
56. Hirokawa Y, Nakajima H, Hanemann CO, Kurtz A, Frahm S, Mautner V and Maruta H. Signal therapy of NF1-deficient tumor xenograft in mice by the anti-PAK1 drug FK228. *Cancer Biol Ther* 2005; 4: 379–381.
57. Wang Y, Lu YF, Li CL, Sun W, Li Z, Wang RR, He T, Yang F, Yang Y, Wang XL, Guan SM and Chen J. Involvement of Rac1 signalling pathway in the development and maintenance of acute inflammatory pain induced by bee venom injection. *Br J Pharmacol* 2016; 173: 937–950.
58. Tan AM, Chang YW, Zhao P, Hains BC and Waxman SG. Rac1-regulated dendritic spine remodeling contributes to neuropathic pain after peripheral nerve injury. *Exp Neurol* 2011; 232: 222–233.
59. Tan AM, Samad OA, Fischer TZ, Zhao P, Persson AK and Waxman SG. Maladaptive dendritic spine remodeling contributes to diabetic neuropathic pain. *J Neurosci* 2012; 32: 6795–6807.
60. Wang SM, Ooi LL and Hui KM. Upregulation of Rac GTPase-activating protein 1 is significantly associated with the early recurrence of human hepatocellular carcinoma. *Clin Cancer Res* 2011; 17: 6040–6051.
61. Nikolic M, Chou MM, Lu W, Mayer BJ and Tsai LH. The p35/Cdk5 kinase is a neuron-specific Rac effector that inhibits Pak1 activity. *Nature* 1998; 395: 194–198.
62. Berg SL, Stone J, Xiao JJ, Chan KK, Nuchtern J, Dauser R, McGuffey L, Thompson P and Blaney SM. Plasma and cerebrospinal fluid pharmacokinetics of depsipeptide (FR901228) in nonhuman primates. *Cancer Chemother Pharmacol* 2004; 54: 85–88.
63. Hansen CN, Fisher LC, Deibert RJ, Jakeman LB, Zhang H, Noble-Haeusslein L, White S and Basso DM. Elevated MMP-9 in the lumbar cord early after thoracic spinal cord injury impedes motor relearning in mice. *J Neurosci* 2013; 33: 13101–13111.
64. Sist B, Fouad K and Winship IR. Plasticity beyond peri-infarct cortex: spinal up regulation of structural plasticity, neurotrophins, and inflammatory cytokines during recovery from cortical stroke. *Exp Neurol* 2014; 252: 47–56.
65. Zhao P, Waxman SG and Hains BC. Extracellular signal-regulated kinase-regulated microglia-neuron signaling by prostaglandin E2 contributes to pain after spinal cord injury. *J Neurosci* 2007; 27: 2357–2368.
66. Zhao P, Waxman SG and Hains BC. Modulation of thalamic nociceptive processing after spinal cord injury through remote activation of thalamic microglia by cysteine cysteine chemokine ligand 21. *J Neurosci* 2007; 27: 8893–8902.
67. Carlton SM, Du J, Tan HY, Nesic O, Hargett GL, Bopp AC, Yamani A, Lin Q, Willis WD and Hulsebosch CE. Peripheral and central sensitization in remote spinal cord regions contribute to central neuropathic pain after spinal cord injury. *Pain* 2009; 147: 265–276.
68. Detloff MR, Fisher LC, McGaughy V, Longbrake EE, Popovich PG and Basso DM. Remote activation of microglia and pro-inflammatory cytokines predict the onset and severity of below-level neuropathic pain after spinal cord injury in rats. *Exp Neurol* 2008; 212: 337–347.
69. Hains BC, Saab CY, Klein JP, Craner MJ and Waxman SG. Altered sodium channel expression in second-order spinal sensory neurons contributes to pain after peripheral nerve injury. *J Neurosci* 2004; 24: 4832–4839.
70. Samad OA, Tan AM, Cheng X, Foster E, Dib-Hajj SD and Waxman SG. Virus-mediated shRNA knockdown of Na(v)1.3 in rat dorsal root ganglion attenuates nerve injury-induced neuropathic pain. *Mol Ther* 2013; 21: 49–56.
71. Waxman SG and Hains BC. Fire and phantoms after spinal cord injury: Na+ channels and central pain. *Trends Neurosci* 2006; 29: 207–215.
72. Ji RR and Strichartz G. Cell signaling and the genesis of neuropathic pain. *Sci STKE* 2004; 2004: reE14
73. Scholz J and Woolf CJ. The neuropathic pain triad: neurons, immune cells and glia. *Nat Neurosci* 2007; 10: 1361–1368.
74. Hayashi K, Ohshima T, Hashimoto M and Mikoshiba K. Pak1 regulates dendritic branching and spine formation. *Devel Neurobio* 2007; 67: 655–669.